AN ABSTRACT OF THE THESIS OF

Gaurav Bhargava for the degree of Master of Science in Electrical and Computer Engineering presented on March 25, 2005.

Title: Via-Only Microwave/Millimeter Wave Bandpass Filters for LTCC Applications

Abstract approved:

Redacted for Privacy

Raghu K. Settaluri

With an increasing number of wireless applications at microwave frequencies, the frequency spectrum is becoming quite crowded. Due to this congestion, the current state of technology is leading towards upper microwave and millimeter wave spectra as they also offer other distinct advantages such as larger bandwidth and smaller component footprint. Low temperature co-fired ceramic (LTCC) has become an enabling technology for a variety of wireless applications at microwave frequencies, as it provides cost-effective, high-density solutions suitable for high-volume production. With the advent of new materials and improved processing techniques, wide range of high quality multi-layered embedded passive components is viable in this technology. Multi chip module (MCM) technology, low-temperature co-fired ceramic (LTCC) has gained extensive popularity over recent years. Interesting features such as tunable dielectric properties, lower dielectric loss and multi-layer realization have given LTCC an edge in the realization of wide-range of embedded passive components. The existing passive component topologies realized in planar configurations such as multi-layered microstrip

and stripline offer effective implementation in LTCC for frequencies up to 20 GHz. Conventionally, for frequencies beyond 20 GHz, conducting waveguide based passive components have distinct advantages over planar counterparts in terms of better insertion losses, lower tolerance sensitivities and availability of wide range of analytical techniques. Application of waveguide concepts to a multi-layered technology such as LTCC, can be quite useful as this can effectively blend in the advantages from both sides to realize new configurations of passive components with improved characteristics. However, as frequency increases, the design complexity increases due to the associated parasitics and one requires accurate analytical procedures combined with effective synthesis techniques for efficient modeling of components to meet a given set of specifications. With a large number of electromagnetic solvers available today, synthesis depends on a tradeoff between time and accuracy. Reduction in synthesis time combined with accurate analysis presents an ideal scenario, which any designer would aspire for.

This work attempts to resolve some of the above mentioned problems by proposing new waveguide based bandpass filter topologies in LTCC. The work focuses on bandpass filter configurations as they are the most popular passive components and are extensively used for a variety of applications. Field theory based accurate analysis combined with impedance-inverter based synthesis techniques have been developed for designing the proposed configurations. The accuracy of the analysis depends on its uniqueness to consider interactions among high order evanescent modes in a rectangular waveguide. The proposed design procedure can be applied to synthesize wide range of waveguide

based bandpass filter configurations. The novelty of these configurations lies in the fact that they can be realized only by using a series of vias. Several issues related to physical realization of these filters are discussed. A detailed sensitivity analysis has been carried out to understand the behavior of the proposed structures. The proposed new filter configurations have been validated with commercially available 3D full-wave electromagnetic simulation tools. This research on new configurations of efficient bandpass filter realization should prove useful for a wide range of applications in the frequency range of 12 to 40 GHz.

Via Only Microwave/ Millimeter Wave Bandpass Filters for LTCC Applications

by

Gaurav Bhargava

A THESIS

submitted to

Oregon State University

In partial fulfillment of
the requirements for the
degree of

Master of Science

Presented March 25, 2005
Commencement June 2005

Master of Science thesis of Gaurav Bhargava presented on March 25, 2005.

APPROVED:

Redacted for Privacy

Major Professor, representing Electrical and Computer Engineering

Redacted for Privacy

Director of the School of Electrical Engineering and Computer Science

Redacted for Privacy

Dean of the Graduate School

I understand that my thesis will become part of the permanent collection of Oregon State University libraries. My signature below authorizes release of my thesis to any reader upon request.

Redacted for Privacy

Gaurav Bhargava, Author

ACKNOWLEDGEMENTS

This is perhaps the easiest and hardest chapter that I have to write. It will be simple to name all the people that helped to get this done, but it will be tough to thank them enough. I will nonetheless try...

I must first thank my advisor Dr. Raghu K. Settaluri for providing invaluable insights, timely encouragement as well as guidance balanced by the freedom to express myself through this work. Throughout my research period, he provided encouragement, sound advice, good teaching, and lots of good ideas. I would have been lost without him.

My special thanks to Prof. Andreas Weisshaar for his insightful discussions. With his enthusiasm, his inspiration, and his great efforts to explain things clearly and simply, helped me in understanding complex electromagnetic problems.

I convey my heartfelt appreciation to my other committee members Dr. Huaping Liu, Dr. Zhongfeng Wang and Dr. Chih-Hung Chang for consenting to be a part of the committee and in lending their valuable suggestions to best convey my research efforts in this manuscript.

My final words go to my family and friends, for all their patience and encouragement. I must therefore thank my fiancée Suruchi for putting up with my late hours, my spoiled weekends, my bad temper, but above all for putting up with me and surviving the ordeal.

My many thanks to Mike, Arien, Shruti and other microwave group colleagues at OSU for their time to time help.

TABLE OF CONTENTS

Page

LIST OF FIGURES

Figure Page

Figure Page

LIST OF TABLES

This work is dedicated to my Grandparents

Onkar and Shail Bhargava

whose motivation and teachings have helped me in all fields of life.

1. INTRODUCTION

Recent advances in integration technology and device performance have paved the way for higher level of System-On-Chip (SOC) or System-In-Package (SIP). On-package components not only miniaturize the module, but also eliminate or minimize the need for discrete components and thereby reduce the assembly time and cost as well. In addition, less discrete components improve reliability due to the reduced solder joint failures. The current drawbacks of most commercially available microwave, millimeter wave, and high-speed optoelectronics transceiver front-ends include the relatively large size and heavy weight primarily caused by discrete components and separately located modules. Multi-layer ceramic and organic-based System-On-Package (SOP) implementation is capable of overcoming this limitation by integrating components that would have otherwise been acquired in discrete form. Integrated passive components on package substrate provide new opportunities to achieve compact hybrid-circuit design in a single package. The System-In-Package (SIP) technology not only provides interconnects to both digital and RF circuits, but also includes a unique feature of building integrated passive components.

With the current expansion of the wireless communication industry, the requirement for high performance filters is increasing. The filters widely used in the front end of RF modules require: compact size, easy fabrication, and low radiation loss. In recent years, compact size and spurious suppression of filter structure are two important factors in any

filter design. Efforts are being made to realize with novel topologies of filters for multi-layer platforms such that they can be embedded on-chip. Zaki *et. al* has reported several on-chip modules for waveguide based bandpass filters and multiplexers recently [1]-[4].

Rectangular Waveguides are one of the conventional transmission lines used to transport microwave signals and are still widely used for a number of applications. They have been used to implement a large variety of microwave components including couplers, isolators, detectors, attenuators and filters for various applications in the frequency range of 1 to 220 GHz. Recently, due to the ongoing efforts to achieve miniaturization and integration waveguide components have been replaced by planar structures such as multi-layered microstrip and stripline configurations.

Inspite of being bulky with high production costs, waveguide components find use at upper microwave and millimeter wave frequencies i.e. above 20 GHz and high power systems due to the compact sizes and better power handling capability. At high frequencies, conducting waveguide based passive components have distinct advantages over planar counterparts in terms of better insertion losses, lower tolerance sensitivities and wide range of analytical techniques. Application of waveguide concepts to a multi-layered technology such as LTCC can be quite useful as this can effectively blend in the advantages from both sides to realize new configurations of passive components with improved characteristics [3], [5], [6].

1.1 LTCC Technology

In this section, a brief introduction about Low Temperature Co-fired Ceramic (LTCC) [7]-[10] is presented. The technology can be defined as a way to produce multilayer circuits with the help of single tapes, which are to be used to apply conductive, dielectric and/or resistive pastes on. These single sheets have to be laminated together and fired in one step all. This saves time, money and reduces circuit dimensions. A major advantage is that every single layer can be inspected and in case of inaccuracy or damage replaced before firing; this prevents the need of manufacturing a whole new circuit. Because of the low firing temperature of about 850°C, it is possible to use the low resistive materials silver and gold instead of molybdenum and tungsten which have to be used in conjunction with the High Temperature Co-fired Ceramic (HTCC). Fig. 1.1 shows a typical LTCC process.

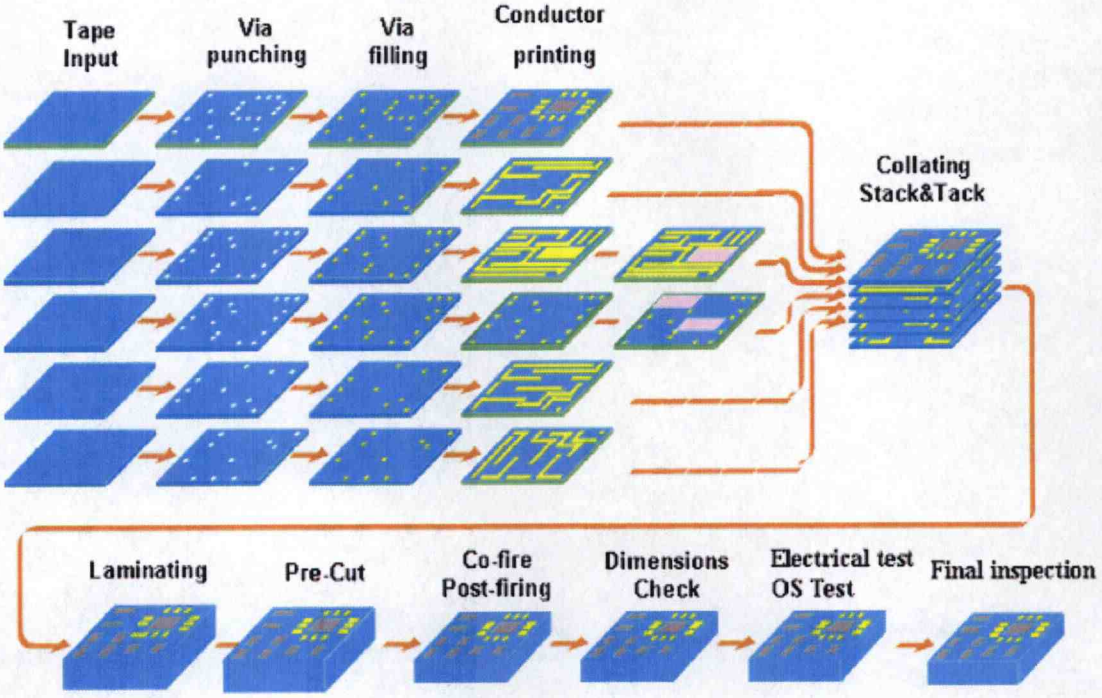

Figure 1.1 A Typical LTCC Process

Low temperature co-fired ceramic (LTCC) is a glass matrix ceramic with crystalline filler added or formed from the glass during the firing process. Since the glass phase of a material is essentially supercooled liquid, it will densify at lower temperatures than the crystalline phase. The crystalline filler is added for thermal expansion match to the semiconductor chip, to control the densification behavior of the LTCC, and to achieve specific electrical performance. This is a significant advantage over crystalline high temperature co-fired ceramic (HTCC) materials which require firing temperature >1600°C. These high temperatures limit the metallization to more refractory, lower conductivity metallization such as tungsten, molybdenum and manganese. These metallization are neither wire bondable nor solder able and therefore require subsequent plating.

Unlike thick film process where successive laminations and firing steps cause bowing and line degradation, the single step lamination and firing of LTCC produces a flat substrate with fine, high quality line definition. In addition, the elimination of costly repeated firings greatly increases the number of conductive layers achievable. The current state of the LTCC technology allows high density circuitry (as fine as 0.002" lines and spaces) interconnected with conductive vias (as fine as 0.0035" diameter). Fig 1.2 shows how LTCC compares in terms of circuit density to other packaging technologies. The wide range in available relative dielectric constant in LTCC increases design flexibility. Relative dielectric constants as low as 3.8 to as high as 20,000 are available. Resistors and capacitors can be realized with these materials. This integration of passive

components [11] reduces the number of surface mount component, reducing the number of solder and wirebond connections, thereby increasing reliability.

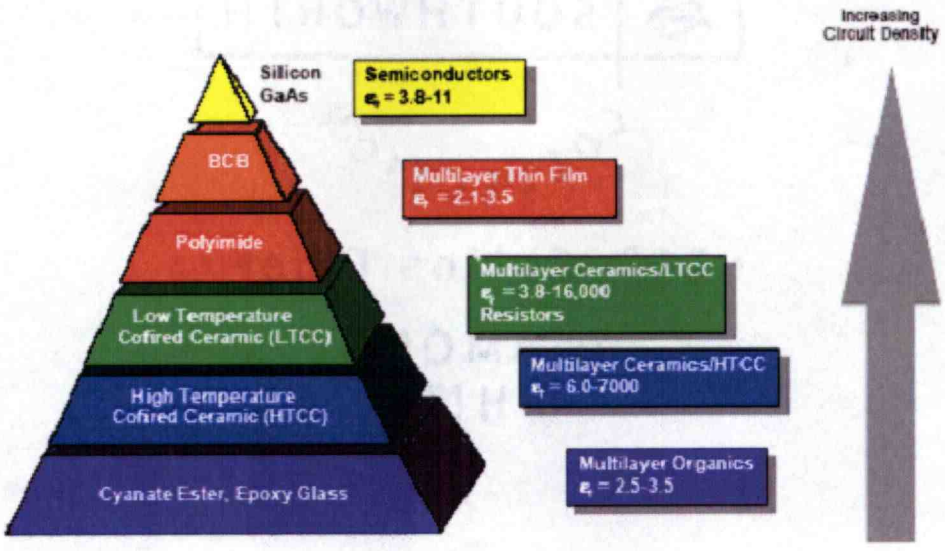

Figure 1.2 Circuit Density Trends in different SOP technologies

The LTCC technology provides many advantages the others do not and offers a couple of benefits:

(1) Fabrication techniques are relatively simple and inexpensive.

(2) Design and manufacture 3-dimesional circuits.

(3) Photo-image processes can be involved into the process steps to increase the circuit accuracy.

(4) Ability to perform frequencies over 30 GHz.

(5) Good thermal stability without degradation during manufacturing and high resistance against ambient working temperatures (up to 350°C)

(6) Lower dielectric loss

The applications of LTCC include:

(1) Applications of high frequencies such as micro-wave, milli-waves

(2) Wireless communication modules

(3) RF passive components such as filter, balun, diplexer, divider and antenna

(4) Optical/power element package

(5) Multi-chip modules require high accuracies

With the advent of new materials and improved processing techniques, wide range of high quality multi-layered embedded passive components is viable in this technology. In the next section, a brief description of a communication system is provided highlighting the advantages of the bandpass filters.

1.2 Typical Communication System

Fig. 1.3 shows a typical communication system with the various components. A brief description is provided to illustrate the advantage of bandpass filters.

At the transmitting end, an information signal is modulated and mixed with a local oscillator to up-convert the carrier frequency. Bandpass filters are used before and after the mixer to stop undesired harmonics. The signal power is amplified before feeding it to the antenna. At the receiving end the entire process is reversed to recover the information. Signal received by the antenna is filtered and amplified to improve the signal-to-noise ratio before feeding it to the mixer for down-converting the frequency. A frequency-selective amplifier (tunable amplifier) amplifies it further, before feeding it to the

demodulator block, which extracts the information signal. At the receiver end, the bandpass filter provides high attenuation to interface signals with low pass band insertion loss.

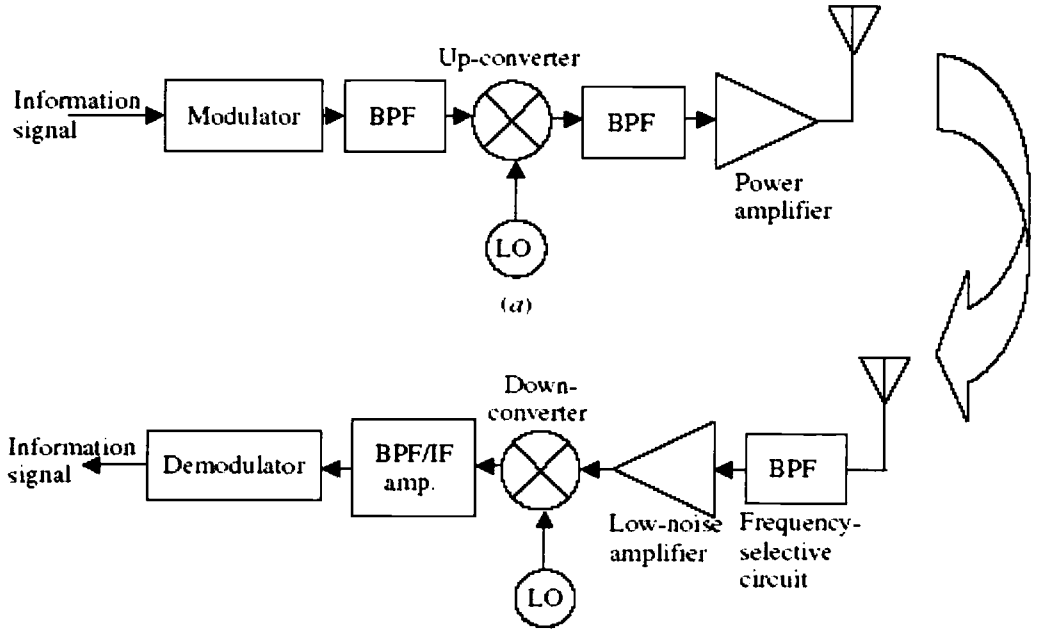

Figure 1.3 A typical Communication System

1.3 Existing technology for a high frequency Bandpass Filter design

Among passive components, bandpass filters are extensively used for a variety of applications. Several variations of bandpass filters such as coupled line filter, interdigital filters, aperture coupled, open loop filters etc have been previously reported in the literature for applications at microwave frequencies [12]-[17]. Multi-layered technologies have been extensively used to achieve miniaturization of filters. The method of folded line bandpass filter propounded by Settaluri *et. al* [18] results in extremely compact

filters with a slightly reduced bandwidth. The use of vialess multi-layer structures has been reported to obtain compact filter geometries [19]-[20]. Other variations such as square stepped impedance resonator on microstrip have been reported to achieve compact footprint [21]. The general assumptions with most of these methods are that they are specific to a certain type of filter.

At upper microwave and millimeter wave frequencies numerous configurations for waveguide bandpass filters have been reported in literature [22]-[28]. Arndt *et. al* [22] – [24] have reported several E-Plane fin-line filters. Vahldieck [25] have reported fin-line and metal insert filters with improved harmonic separation and increased stopband characteristics featuring symmetric step discontinuities at input and output. The tunability aspect of waveguide e-plane filters has been well covered by Budimir [26]. Several other filter topologies consisting of an inductive window has been reported [27], [28].

Critical inherent advantages of waveguide based passive components over planar counterparts have generated great interest among researchers to realize waveguide in multi-layered configurations [29]. Laminated waveguide, as introduced by Uchimura *et.al* [29] have been used to realize bandpass filters for LTCC technologies [30]. Additionally, these structures can be efficiently transitioned to other transmission line structures such as microstrip or striplines [31], [32]. A typical bandpass filter response is shown in Fig. 1.4.

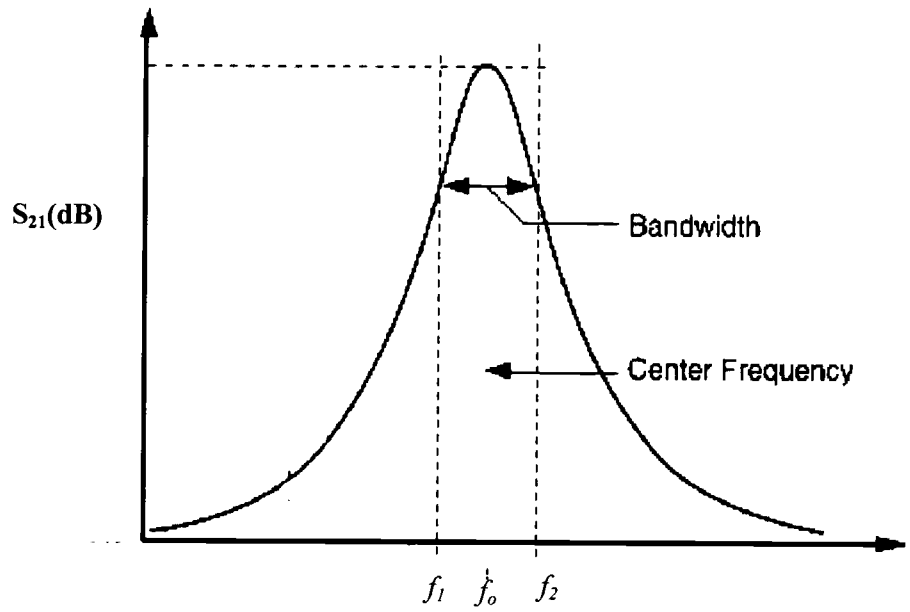

Figure 1.4 Bandpass filter response

Here f_0 is the center frequency and $f_2 - f_1$ is the bandwidth.

The ideal bandpass filter provides infinite stopband attenuation and no passband loss. Depending on the response of the filters in the passband and stopband, they can be characterized as maximally flat (Butterworth) filters and equi-ripple (Chebyshev) filters.

1.4 Design Techniques

With more and more applications shifting to upper microwave and millimeter wave frequencies, accurate design of bandpass filters is one of the critical factors that is currently faced by several researchers. The design techniques proposed in [22]-[24] suffer from some inherent disadvantages such as the designed filter topologies have poor physical tolerances. With a large number of iterative variables, i.e. the lengths of each filter element, the design procedure is complex and is restricted in its application to lesser

number of resonator section filters. Most importantly, as the optimization process is targeted at obtaining a desired frequency response by varying lengths of filter elements, the obtained lengths might be extraordinarily large or small in some cases which are highly undesirable as it might cause concerns for physical realization.

With a large number of Electromagnetic (EM) simulators available commercially today, full wave simulation has become an indispensable tool in design of circuits at upper microwave and millimeter wave frequencies. Though, while using electromagnetic simulators there exists a tradeoff between accuracy and computational time. Thus, their use is undesirable though unavoidable.

Reduction in synthesis time combined with accurate analysis presents an ideal scenario, which any designer would aspire for. In this work field theory based accurate analysis combined with impedance-inverter based synthesis techniques have been developed for designing the proposed configurations. The accuracy of the analysis depends on its uniqueness to consider interactions among high order evanescent modes in a rectangular waveguide. The proposed design procedure can be applied to synthesize wide range of waveguide based bandpass filter configurations.

1.5 Organization of the thesis

The focus of research was to develop new configurations of *waveguide based filters for LTCC applications* at microwave and millimeter wave frequencies. The filters have been analyzed using field theory with an aim to develop a comprehensive method of designing

waveguide filters. The new configurations are based on filter-sections with dominant inductive and capacitive coupling to provide superior bandpass filter performance.

In chapter 2, the theory and design equations underlying bandpass filter designs are presented. An overview of conventional design procedure for waveguide bandpass filters is discussed before the impedance inverter approach is introduced. This enables the readers to appreciate the simplicity of the new technique. A brief study of electromagnetic simulators is presented with an application to waveguide based geometries.

In chapter 3, a new class of inductive-iris waveguide bandpass filters is presented for LTCC applications. A rigorous field theory analysis of the proposed filter topologies has been carried out. The impedance inverter network has been used to design bandpass filters with different specifications and their frequency response is presented. Full wave electromagnetic simulations in Ansoft High Frequency Structure Simulator [33] have been carried out to validate the theory. Finally a footprint comparison has been provided for the designed filters demonstrating the adaptability of the filters for multi-layered environment.

Chapter 4 presents the design issues concerning the implementation of via-only E-Plane metal insert filters on multi-layer substrates with improved stopband characteristics. Several studies have been reported to realize compact filter topologies. The designed filters have been simulated with the three dimensional electromagnetic solvers in multi-

layer configurations. Several designs with footprint layouts have been presented to demonstrate the concept.

Chapter 5 summarizes the work in this thesis and puts forth recommendations for future work based on the viability of the proposed design technique to other waveguide components used at higher frequencies.

2. FILTER DESIGN THEORY

The ever decreasing bandwidth for various wireless applications in the lower frequency bands (1-10 GHz) have created a shift to less crowded higher frequency bands such as Ka and Ku to meet the bandwidth requirements. At microwave/ millimeter-wave frequencies, the lumped element design using inductors and capacitors is no longer feasible due to the distributed nature of the transmission lines and increased parasitic effects. These effects are predominant as the size of element becomes comparable to a fraction of a wavelength. This chapter presents an overview of the relevant filter design theory applicable for microwave/ millimeter-wave frequencies. Section 2.1 explains the concept of impedance inverters, with reference to filter design. Section 2.2 presents the conventional filter design technique for a general bandpass filter. Section 2.3 presents the filter design approach using impedance inverters. Section 2.4 covers a brief introduction about High Frequency Structure Simulator, a 3D electromagnetic simulator from Ansoft Inc. [33].

The two existing approaches to design of filters are a) image parameter method and b) insertion loss method. The image parameter method is relatively simple but lacks in the capability to specify the frequency response. Thus, to obtain filters with desired response several iterations have to be carried out. On the other hand, the insertion loss method is a more recent approach based on network synthesis. The filters can be designed with a completely specified frequency response.

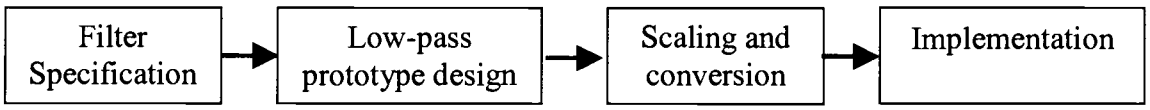

Figure 2.1 Filter design by Insertion Loss Method [34]

Fig. 2.1 shows a block diagram for filter design process using insertion loss method. In insertion loss method, the design begins with setting up the specifications for the filter. The filter specifications are: the number of resonator sections (N), type of filter (Maximally flat or Chebyshev), passband ripple (if applicable), fractional bandwidth required for the filter, desired insertion loss at any frequency [34]. Using a set of filter specifications, the lowpass prototype as shown in Fig. 2.2 is constructed.

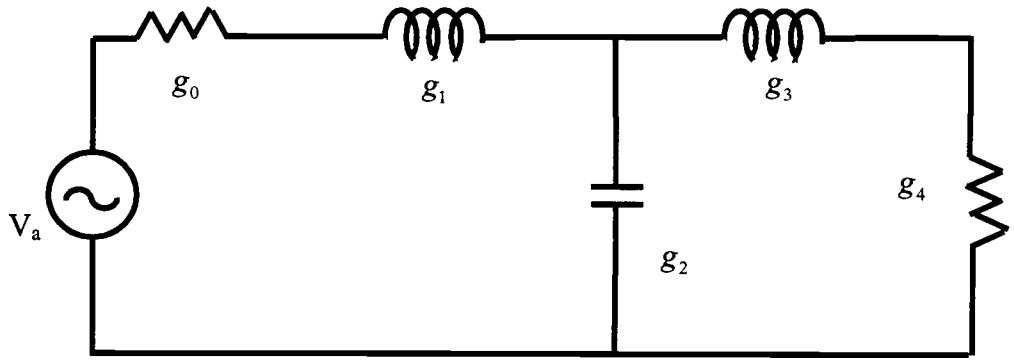

Figure 2.2 Lowpass Prototype for a 3rd order filter

These prototype values are denoted as g_s for normalized values of frequency and impedance. Thus for a 4th order filter, the element values are numbered from g_0, at the generator impedance, to g_{n+1} i.e. g_5 at the load impedance. The network elements alternate between series and shunt connections depending on g_0 being a resistance or conductance. These values are unique to a given set of specifications and can be obtained

from the standard tables [34] available. The prototype then can be scaled and converted to obtain a desired response using the standard techniques. As both image parameter method and insertion loss method give a lumped element design, their application to distributed networks needs further transformations. The transformation can be carried out using Richard's transformation [34] and Kuroda identities [34]. The impedance inverter network approach for designing bandpass filters is based on inductive coupling between filter sections and is explained in the following section.

2.1 Impedance Inverter Network

An impedance inverter network can be constructed using quarter wave transmission lines placed before load impedances. Quarter wave lines when used in specific network configurations convert shunt elements to series and vice versa. The impedance inverters or K-inverters form the basis of the filter design procedure and have been explained in detail. Figure 2.3 shows the K-inverter network using a quarter-wave line and its alternative implementation.

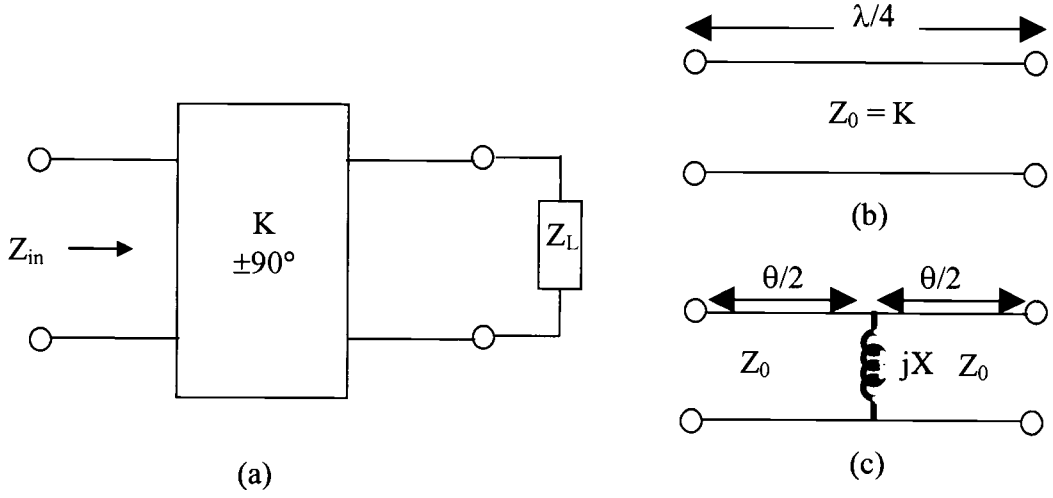

Figure 2.3 (a)-(c) Impedance inverter and its alternate implementations.

For the impedance inverter as shown in 2.3 (a)

$$Z_{in} = \frac{K^2}{Z_L} \tag{2.1}$$

For the 90° line as in Fig. 2.3 (b)

$$K = Z_0 \tag{2.2}$$

For the lumped element implementation in Fig. 2.3 (c)

$$K = Z_0 \tan\left|\frac{\theta}{2}\right| \tag{2.3a}$$

$$X = \frac{K}{1-\left(\frac{K}{Z_0}\right)^2} \tag{2.3b}$$

$$\theta = -\tan^{-1}\frac{2X}{Z_0} \tag{2.3c}$$

The transmission line lengths θ/2 normally negative but in design procedure here, it would be absorbed as a part of the resonator sections as explained in the forthcoming sections.

2.2 Conventional Filter design

The conventional design approach to implement inductive coupled bandpass filters is:

- Shunt Inductance Coupled waveguide filters

The first step to design the waveguide filter is to make the equivalent circuit from the normalized lowpass filter as shown in Figs. 2.2 and 2.4. The next step is to change a LC-resonator to the cavity resonator and change a coupling inductor to the posts [34].

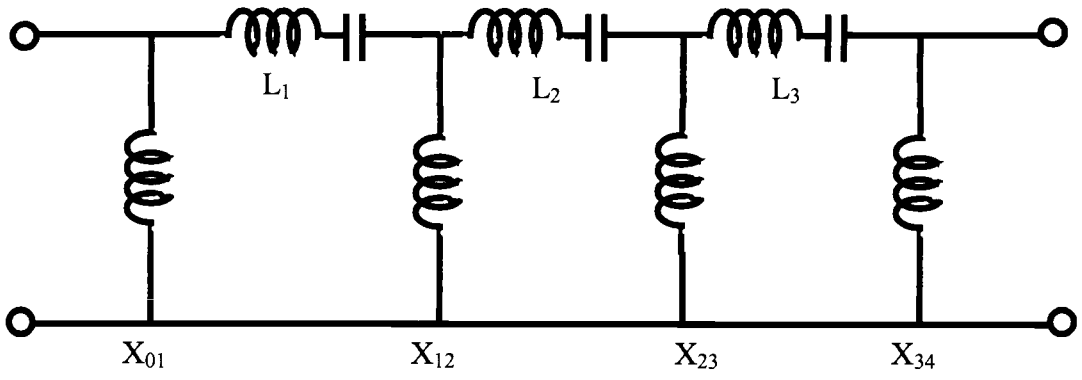

Figure 2.4 Bandpass Filter as scaled from lowpass prototype [34]

The procedure to change the waveguide filter from the normalized low pass filter is shown below. Bandpass filter (BPF) is obtained from the lowpass filter (LPF). Each part is changed into the structure of the waveguide filter as followings; The changing parameters

are $g_0, g_1 \rightarrow X_{01}, g_1, g_2 \rightarrow X_{12}, g_2, g_3 \rightarrow X_{23}, g_3, g_4 \rightarrow X_{34}, X_{01}, X_{12} \rightarrow L_1, X_{12}, X_{23} \rightarrow L_2$, $X_{23}, X_{34} \rightarrow L_3$. Where g_0, g_1, ….,g_{n+1} are the lowpass filter prototype values and X_{01}, X_{12}, X_{23}, X_{34} are the shunt reactance's for lumped inductance discontinuities. Element values can be obtained as

$$K_{0,1} = \sqrt{\frac{\pi}{2}\frac{\omega_\lambda}{g_0 g_1}} \tag{2.4a}$$

$$K_{j,j+1} = \frac{\pi\omega_\lambda}{2}\sqrt{\frac{1}{g_{j-1}g_j}} \quad j:1\sim n-1 \tag{2.4b}$$

$$K_{n-1,n} = \sqrt{\frac{\pi}{2}\frac{\omega_\lambda}{g_{n-1}g_n}} \tag{2.4c}$$

where $K_{j,j+1}$ are the impedance inverter parameters, ω_λ is the guide-wavelength fractional bandwidth and is calculated as follows:

$$\omega_\lambda = \left(\frac{\lambda_{g0}}{\lambda_0}\right)^2 \left(\frac{\omega_2 - \omega_1}{\omega_0}\right) \tag{2.5}$$

$$X_{j,j+1} = \frac{K_{j,j+1}}{1 - K_{j,j+1}^{\ 2}} \quad j: 0 \sim n-1 \tag{2.6}$$

$$\theta_j = \pi - \frac{1}{2}\left[\tan^{-1}(2X_{j-1,j}) + \tan^{-1}(2X_{j,j+1})\right] rad \quad j: 1 \sim n-1 \tag{2.7}$$

$$L_j = \frac{\theta_j \lambda_{g0}}{2\pi} \tag{2.8}$$

where,

λ_{g0} : guide wavelength of the waveguide

λ_0 : wavelength at center frequency in free space

θ_j : $X_{j,j+1}$ Phase length in the waveguide

L_j : Resonator length

The length of each resonator can be decided from equation (2.8). The width of iris inside the waveguide can be decided from equation (2.4). Relation between the equation (2.4) and the width of iris are based on Marcuvitz curve [35].

2.3 Bandpass filter design using impedance inverter approach

The simplicity of the impedance inverter approach gives it a wide spread application in design of bandpass filters. The approach as is based on the network model of the section

does not affect physical configuration of the section and is applicable to any type of bandpass filter section.

Fig 2.5a shows a second order inductively coupled waveguide filter. Fig. 2.5b and 2.5c show a filter section and its equivalent impedance inverter (K-inverter) network respectively. Fig. 2.5d shows a cascaded network with two filter sections. The first step to realize the filter is to determine the reactance parameters of the filter section shown in Fig. 2.5c. This can be carried out by dividing the filter section into a set of known geometries as indicated in the figure and then combining the individual scattering parameters to obtain the final S parameters of the section.

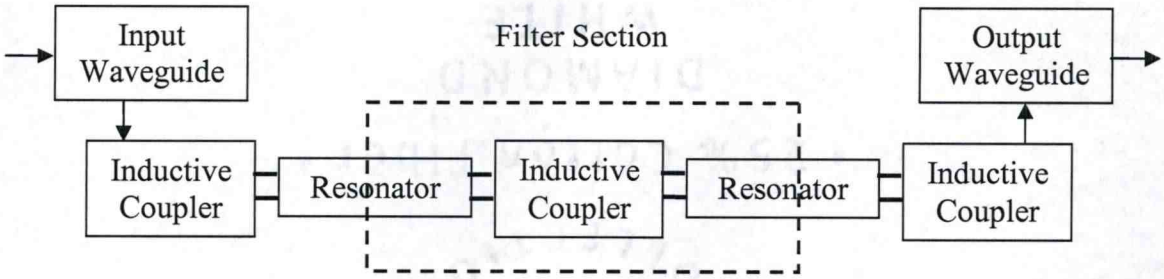

(a) A 2nd order inductively coupled filter

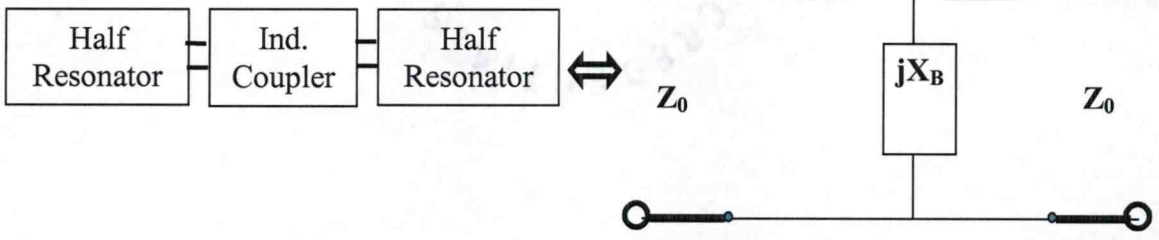

(b) A single filter section

(c) Equivalent K-inverter network

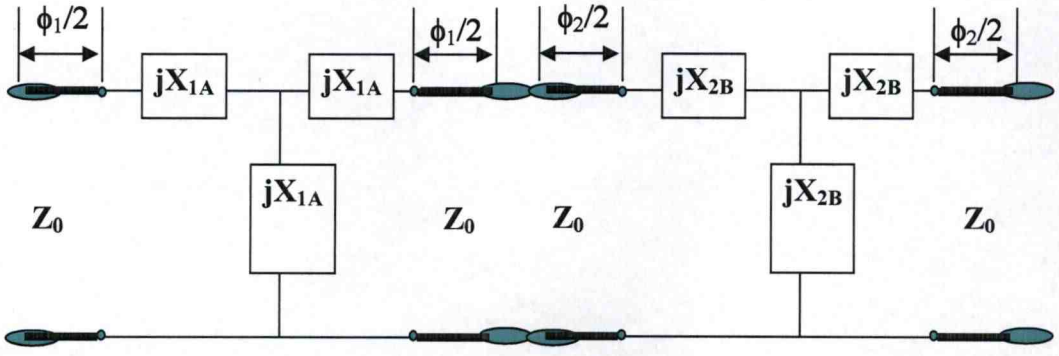

(d) Cascaded Network with two filter sections

Figure 2.5 Filter representation with impedance inverter approach

The next step is to represent each filter section in terms of a T-equivalent impedance inverter parameter network as shown in Fig. 2.5c. For symmetrical sections (such as the one shown in Fig 2.5b, the network shown in Fig 2.5c will be identical to the filter section, provided the K and ϕ are given by the equation (2.9)

$$\phi = -\tan^{-1}\left(2X_b + X_a\right) - \tan^{-1}\left(X_a\right) \tag{2.9a}$$

$$K = \left|\tan\left(\frac{\phi}{2} + \tan^{-1}\left(X_a\right)\right)\right| \tag{2.9b}$$

Bandpass filters are realized by cascading the individual sections synthesized by the procedure shown above. It is of significance that when the sum of the interconnecting lengths between two T networks is $-\pi$. The length of the resonator between the two sections is zero in accordance to equation 2.8. Thus, the filter consists of cascaded sections with no additional resonator lengths between, thereby making the structure extremely compact.

2.4 High Frequency Structure Simulator by Ansoft Inc [33].

High Frequency Structure Simulator (HFSS) has been used to validate the theoretical results for all the filter designs. HFSS v9.2 is a product from Ansoft Corporation and has the capability to carry out 3D Electromagnetic Simulations for arbitrary geometries. All the waveguide components have 3D geometries and can not be analyzed using 2D and 2.5D simulators.

HFSS analyzes the waveguide 3D structure using Finite Element Method (FEM) which provides it the unique advantages such as automatic fine refinement and small details in a larger problem space can be resolved easily. Where, there is a compromise on the simulation time.

In this section, a brief overview has been provided on the settings of various simulation parameters.

1. Mesh Control:

   The way HFSS discretizes the mesh is it breaks the structure into small tetrahedrons. The mesh is finer at the boundaries as compared to center. To obtain accurate simulation results the mesh structure should also be finer in the center of the waveguides. Lambda Refinement and refinement per pass are the two important parameters that need to be specified in order to obtain finer mesh structures. Here pass refers to an adaptive pass which is a unique feature to FEM simulators and allows them to refine mesh on basis on error functions. A higher number of adaptive passes are needed to converge to the correct solution with the default settings. As we guide the software in the meshing process we need to consider geometrical resolution, guide wavelength and spatial wavelength. The geometrical solution we use for various objects in the model is a trade-off between accuracy and solution time. Starting with a realistic lambda based starting mesh helps the software sample the problem based on the guide wavelength.

Table 1 shows results from a study that was conducted to determine correct set of values for all these variables in order to get fast and accurate results. The decision criteria are the number of tetrahedrons and convergence of the scattering parameters. It may be seen that the larger the number of tetrahedrons the better, but a tradeoff between simulation time and number of tetrahedrons has to be established to obtain faster response. The simulation time increases nonlinearly with the number of tetrahedrons.

Table 1 Number of Tetrahedrons

No.	*Number of Adap. Passes*	*Lambda Refinement*	*% change per pass*	Number of tetrahedrons
1	2	0.3333	20	1254
2	4	0.25	30	9154
3	6	0.25	30	13238
4	2	0.1	40	22744

KEY POINTS

- solution frequency for filters should be observed to be as the center frequency.
- Lambda refinement should be set anywhere between 0.15 – 0.25.
- Refinement per pass should be set between 25% - 35%
- Maximum number of passes to be set to 5-6. It depends on the convergence for the results. It may be required to run a couple of simulations to determine the right number of passes.
- While carrying out a frequency sweep, interpolation method is preferred for faster results. Discrete method is suggested for fewer solution frequency points

3. VIA-ONLY INDUCTIVE IRIS WAVEGUIDE BANDPASS FILTERS

In this chapter, novel via-only inductive iris bandpass filters will be presented. The proposed concept of via-only bandpass filters is based on the inductive-iris waveguide filters [27]. Fig. 3.1a and 3.1b, show a conventional rectangular waveguide and the corresponding implementation in a dielectric substrate using vias respectively. The two side walls connecting the top and bottom conducting layers are realized by using through vias separated by the broadside width of the waveguide, *a*. The dielectric thickness is kept same as the height of the waveguide, *b*. Fig. 3.1c shows a three-resonator implementation of the filter in the dielectric-loaded configuration with conducting side walls replaced by a series of vias. The resonator sections are inductively coupled by reduced width waveguides of different widths depending on the order of coupling [27]. A typical filter section consists of two half-resonator sections separated by a reduced-width waveguide section as shown in Fig. 3.1d and the corresponding impedance inverter equivalent circuit is given in Fig. 3.1e. The next section demonstrates the viability of having a series of vias for sidewall in a waveguide. The following sections explain the full-wave analysis of the filter section and the K-inverter parameter approach for the filter synthesis.

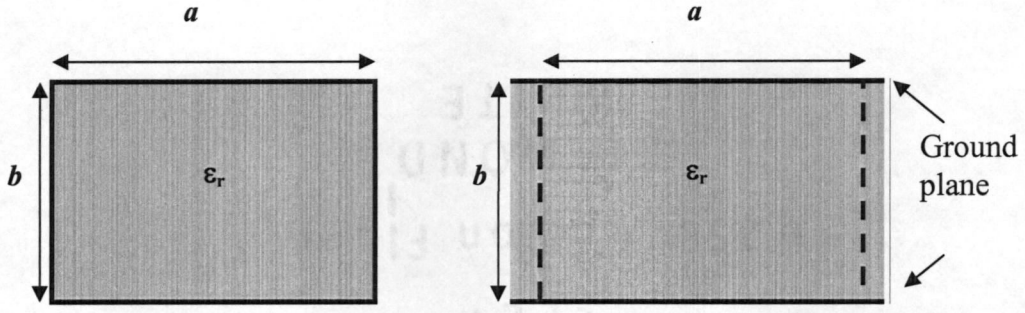

(a) Conventional Waveguide (b) Waveguide formed using vias

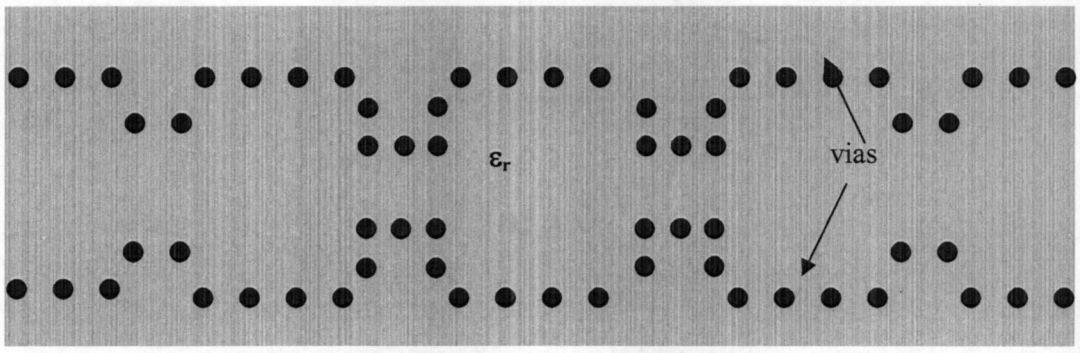

(c) Top view of the proposed filter

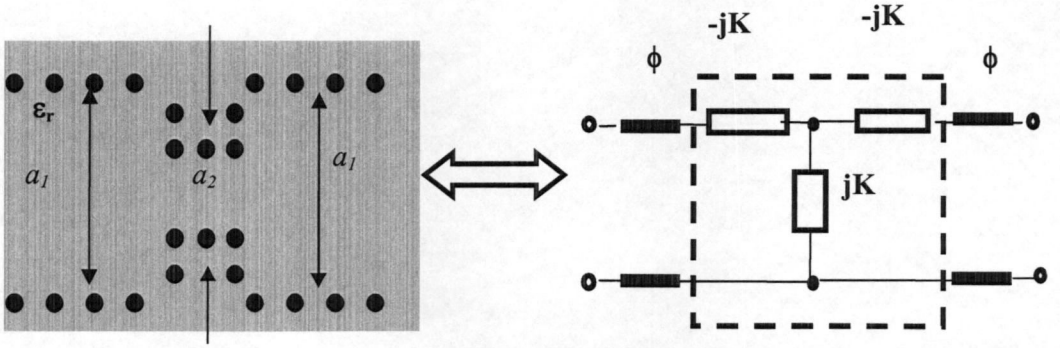

(d) Single filter Section

(e) Impedance Inverter Equivalent circuit

Figure 3.1 Proposed Via-Only Filter. (a) Conventional Waveguide (b) Waveguide formed using vias (c) Top view of the proposed filter (d) Single filter Section (e) Impedance Inverter Equivalent circuit

3.1 Conventional Waveguide and Waveguide with Sidewalls as Series of Vias

The proposed filter consists of inductive iris waveguides resonators with their sidewalls replaced by a series of vias. Inductive iris waveguide filters have been reported in the past, but the new approach of having a series of vias to replace the sidewalls can be helpful in realizing embedded topologies for waveguide passive components in multi-layer technologies. Thus an understanding of electric and magnetic field transmission along the two waveguides will help in answering questions pertaining to via size and placement. In this section the results from a study carried out to understand effect on magnetic and electric fields in the two waveguide topologies as shown in Fig. 3.2c and 3.2d are discussed.

Fig 3.2a and 3.2b, show a cross section of a conventional rectangular waveguide and the corresponding implementation in dielectric loaded platform using vias respectively in the V band. Fig. 3.2c and 3.2d show the three dimensional view of a rectangular waveguide and a waveguide with sidewalls replaced with a series of vias respectively. The two side walls connecting the top and bottom conducting layers are realized by using through vias separated by the broadside width of the waveguide, a. The dielectric thickness is kept same as the height of the waveguide. The structure is simulated in HFSS at a frequency of 60GHz, for a waveguide of length 3mm and effective dielectric constant is 5 [29].

Fig. 3.3 shows the radiation of magnetic field vector as seen from the top view of the three dimensional structure shown in Fig. 3.2d. Fig 3.3a shows the magnetic field vector

in a conventional rectangular waveguide. The magnetic field is maximum at the boundaries and minimum in the center.

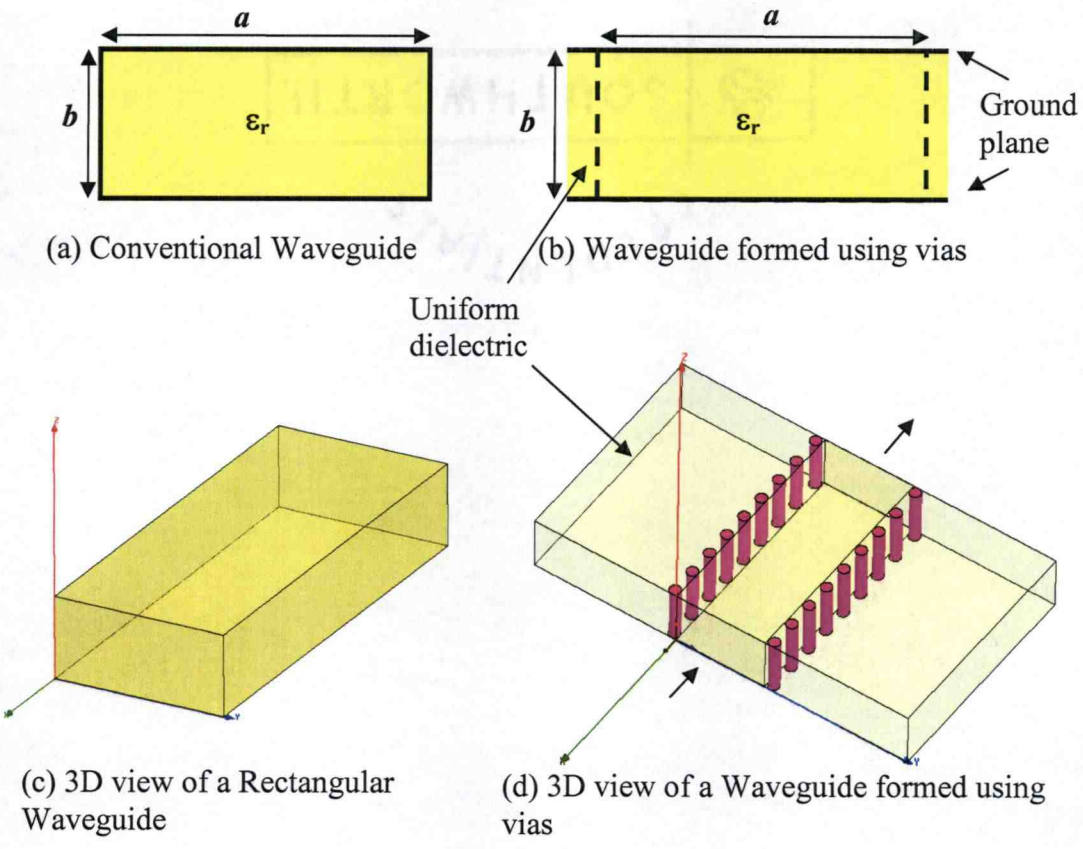

(a) Conventional Waveguide

(b) Waveguide formed using vias

(c) 3D view of a Rectangular Waveguide

(d) 3D view of a Waveguide formed using vias

Figure 3.2 Demonstration of waveguide implementation in multi-layer configurations

Fig 3.3b is the vector plot of magnetic field in the dielectric for a waveguide implemented with a via fence. Solid vias with diameter of 150μm and a pitch of 220μm have been used to realize the via fence. Pitch is the distance between the centers of two consecutive vias. As can be seen, the magnetic field is confined within the series of vias and there is no radiation into the substrate. It can be attributed to as the diameter and spacing of the vias is much shorter than the operating wavelength and therefore is equivalent to a conducting wall. Fig 3.3c and 3.3d show an increase in radiation through the via fence into the

substrate with an increase in pitch. It can be seen that using a series of via with a smaller pitch maintains the same magnetic field in the region of interest when compared to the conventional dielectric filled rectangular waveguide.

Fig. 3.4 shows the effect on electric field vector with changing pitch. Fig. 3.4a shows the electric field vector as seen from left for a conventional rectangular waveguide. It may be seen that an increase in via separation from Fig 3.4b – Fig. 3.4d shows a shift in the effective guide wavelength of the waveguide. No radiation is observed in the electric field as the waveguide is excited in the dominant TE_{10} mode. TE_{10} mode refers to zero magnitude of electric field at the boundaries and peak in center of the waveguide. It may be seen that there is negligible shift in guide wavelength for smaller values of pitch. The effect is similar to what has been observed with the magnetic field vector. Thus it can be concluded that a series of vias with small pitch can be used to realize a conventional rectangular waveguide in dielectric substrates.

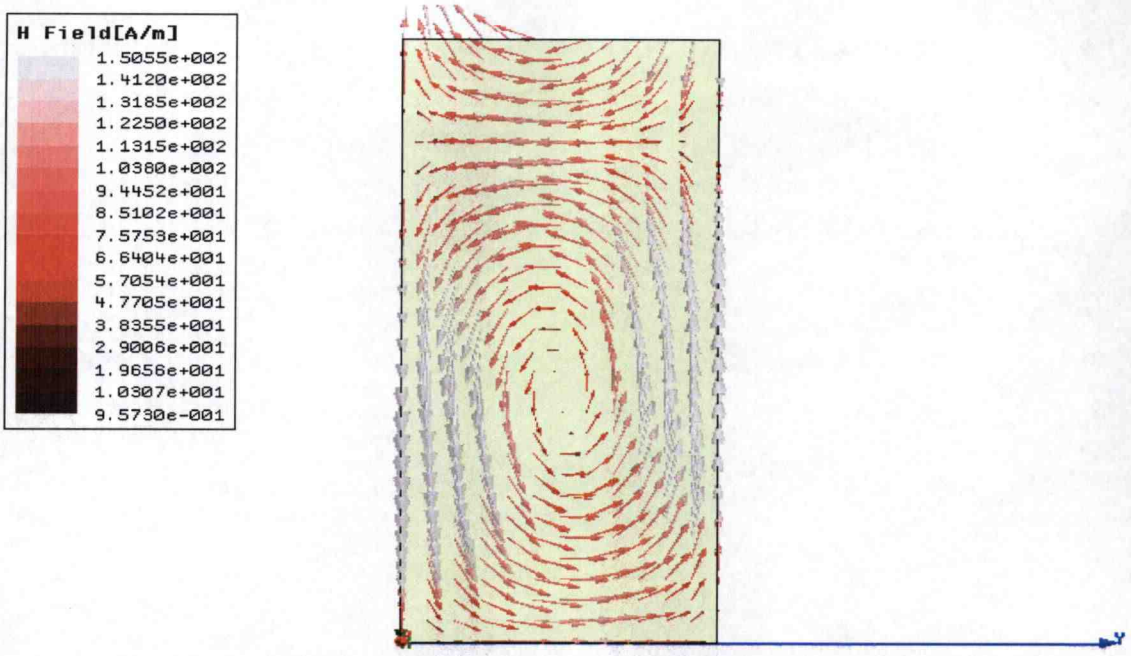

(a) Top view of a conventional rectangular waveguide demonstrating magnetic field vector inside the cavity

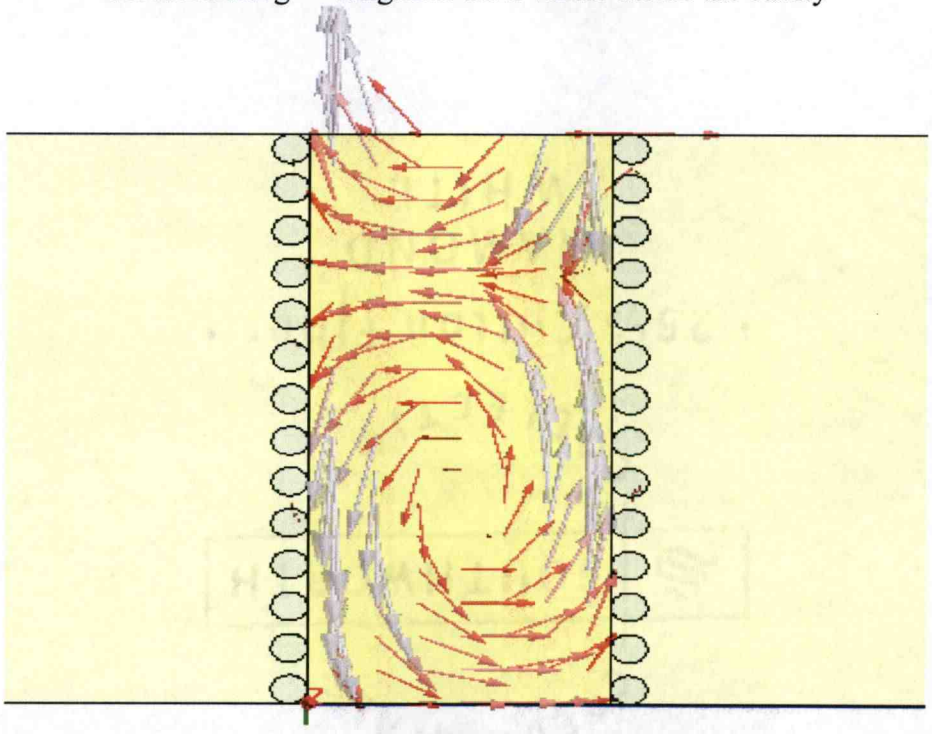

(b) Top view of a waveguide, with via fences as sidewalls showing magnetic field vector in the dielectric. Pitch = 220μm, $Via_{diameter}$ = 150μm

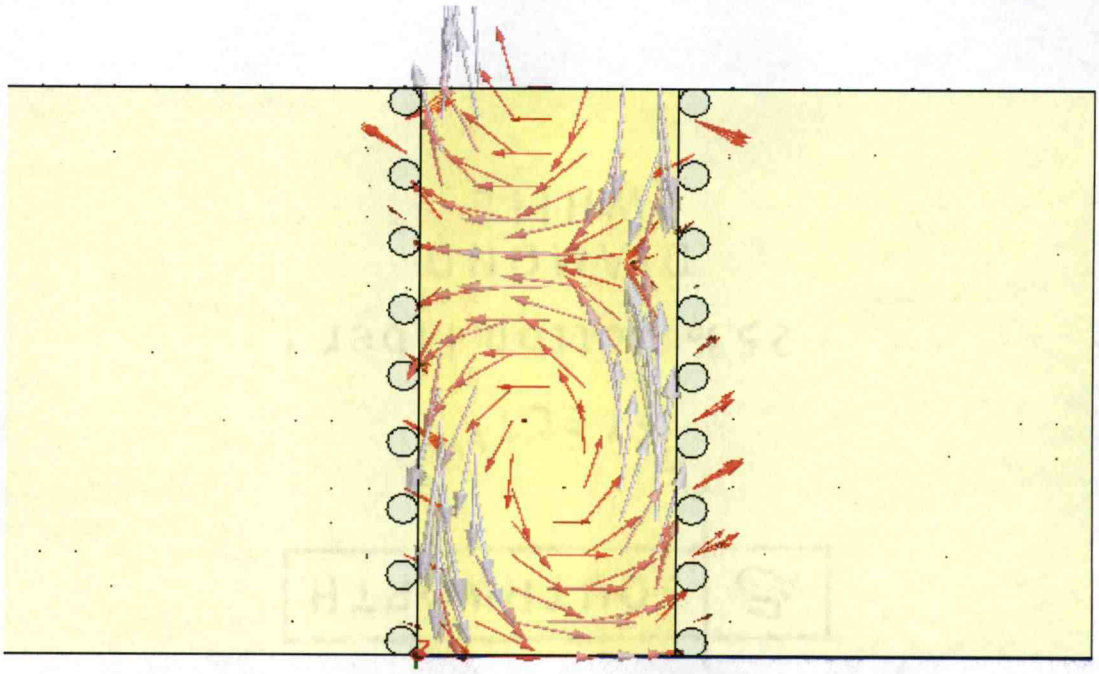

(c) Top view of a waveguide, with via fences as sidewalls showing magnetic field vector in the dielectric. Pitch = 350μm, $Via_{diameter}$ = 150μm

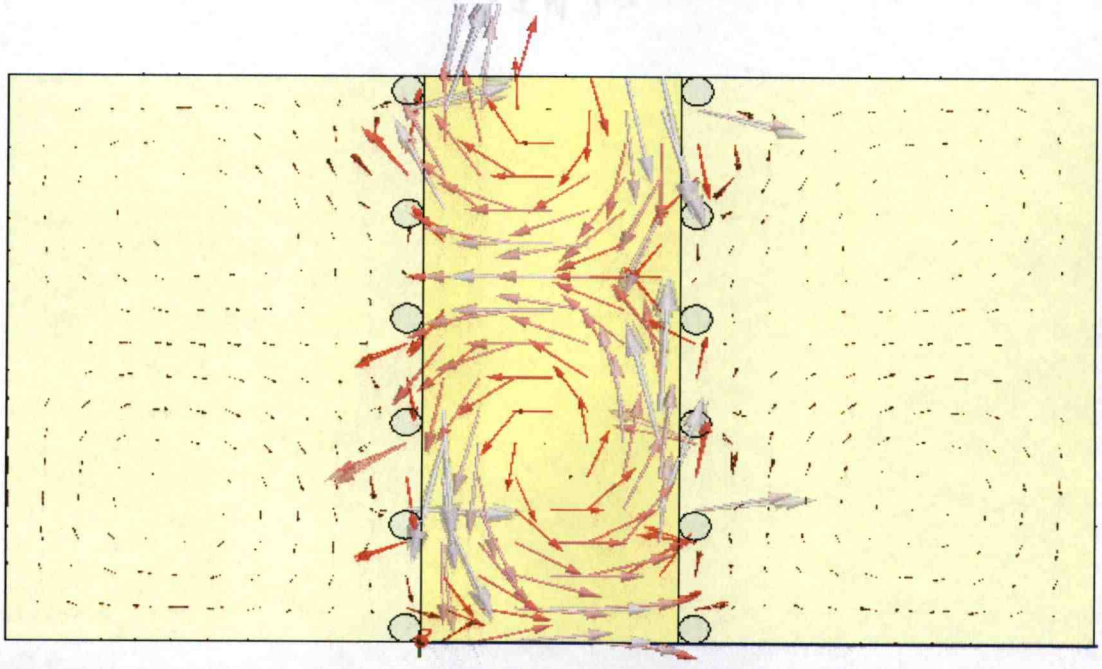

(d) Top view of a waveguide, with via fences as sidewalls showing larger radiation of magnetic field vector in the dielectric. Pitch = 550μm, $Via_{diameter}$ = 150μm

Figure 3.3 Magnetic field vector plots for via fence waveguide realizations with varying pitch.

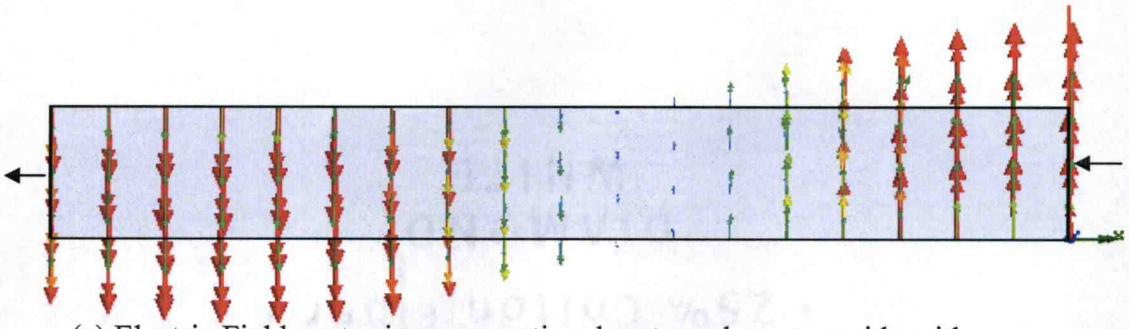

(a) Electric Field vector in a conventional rectangular waveguide with continuous conducting boundaries on sidewalls

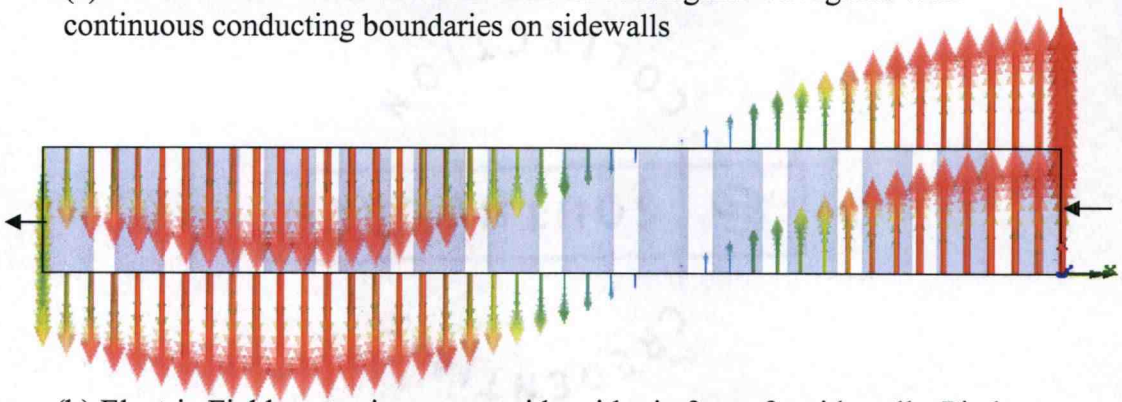

(b) Electric Field vector in a waveguide with via fence for sidewalls. Pitch = 220μm

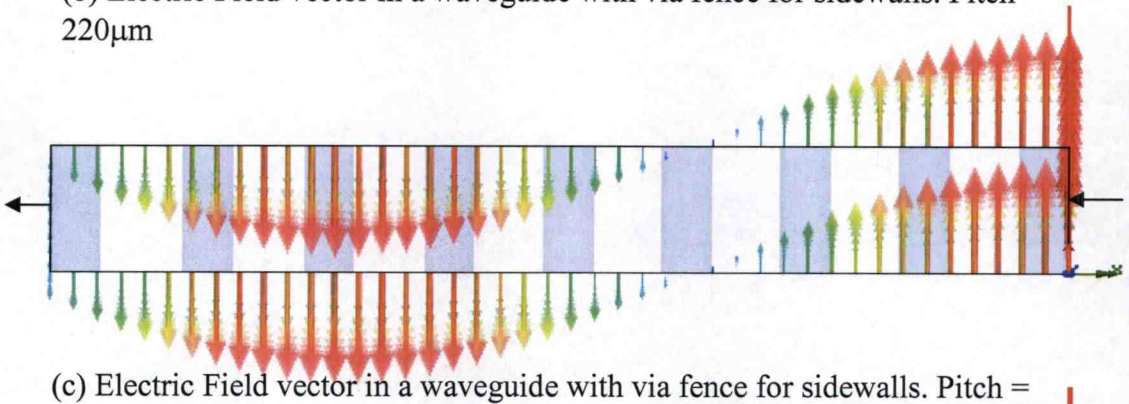

(c) Electric Field vector in a waveguide with via fence for sidewalls. Pitch = 350μm

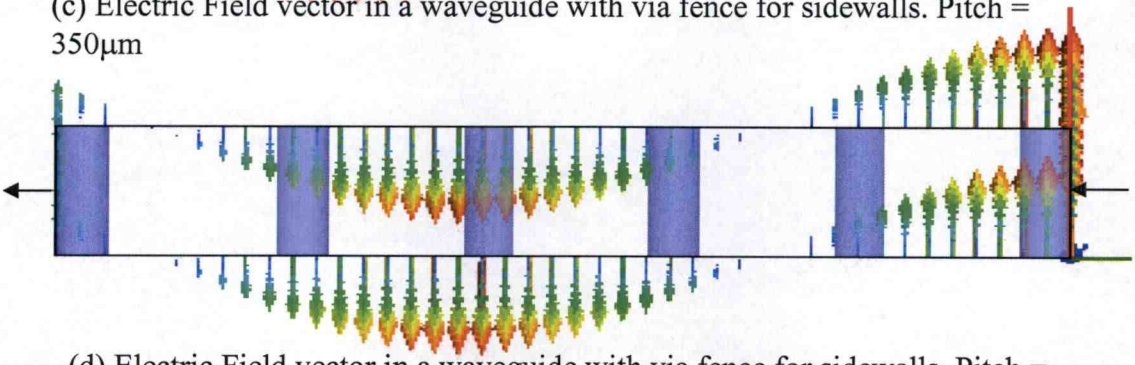

(d) Electric Field vector in a waveguide with via fence for sidewalls. Pitch = 550μm

Figure 3.4 Electric Field as seen from Side View for various configurations. Red shows peak amplitude as compared to blue being the least.

3.2 Elements of a Waveguide Inductive Iris Filter Section

A hollow rectangular waveguide does not support TEM waves, since only one conductor is present. Only TM or TE modes can propagate in a rectangular waveguide. The TM and TE modes of a waveguide have cutoff frequencies, below which propagation is not possible. Transverse Electric (TE) modes are characterized by fields with $E_z = 0$ while H_z must satisfy the reduced wave equation

$$\left(\frac{\partial^2}{\partial x^2}+\frac{\partial^2}{\partial y^2}+k_c{}^2\right)h_z(x,y)=0 \tag{3.1a}$$

with

$$H_z(x,y,z)=h_z(x,y)\exp(-j\beta z) \tag{3.1b}$$

and $k_c{}^2=k^2-\beta^2$ is the cutoff wavenumber.

Transverse Magnetic (TM) modes are characterized with $H_z = 0$ while E_z must satisfy the reduced wave equation:

$$\left(\frac{\partial^2}{\partial x^2}+\frac{\partial^2}{\partial y^2}+k_c{}^2\right)e_z(x,y)=0 \tag{3.2a}$$

with

$$E_z(x,y,z)=e_z(x,y)\exp(-j\beta z) \tag{3.2b}$$

and $k_c{}^2=k^2-\beta^2$ is the cutoff wavenumber.

This section characterizes a waveguide on the basis of its cutoff frequency, propagation constant and impedance.

The cutoff frequency, propagation constant and impedance of a rectangular waveguide can be determined as follows:

Each m-n pair describes one solution set named as the mode-mn. β is the propagation constant given as

$$\beta mn = \sqrt{\omega^2 \mu\varepsilon - k_{cmn}{}^2} = 2\pi\sqrt{\mu\varepsilon}\sqrt{f^2 - f_{cmn}{}^2} \tag{3.3a}$$

where

$$k_{cmn} = \frac{1}{2}\sqrt{(m/a)^2 + (n/b)^2} \tag{3.3b}$$

and f_c is the cutoff frequency of the relevant mode given as

$$f_{cmn} = \frac{1}{2\sqrt{\mu\varepsilon}}\sqrt{(m/b)^2 + (n/a)^2} \tag{3.3c}$$

where a and b are respectively the width and height of a rectangular waveguide, ε_r and μ are the dielectric constant and permeability of the medium. It is clear that propagation constant β is real for $f>f_c$. That is, the signal propagates for $f>f_c$ while it attenuates exponentially for $f<f_c$. For TE_{mn} modes, characteristic wave impedance is defined as follows:

$$Z_{wmn} = \frac{\sqrt{\mu/\varepsilon}}{\sqrt{1-(f_{cmn}/f)^2}} \tag{3.3d}$$

Depending on the frequency of the signal and the transversal dimensions of the waveguide, the power fed to the waveguide may be split into various modes described above to travel to the output port. Splitting of the power into different modes is usually undesirable because each mode may travel with different velocity leading to dispersion. Further, in order to have efficient power transfer to and from the waveguide, special transitions must be used, optimized for a certain mode. For these reasons in practice a

single mode of operation is desirable. This is possible if the frequency is selected to be above the lowest cutoff frequency and below the second cutoff frequency. This mode is named as dominant mode. For $b<a$ the dominant mode is TE_{10} (m=1, n=0) mode because it has the lowest cutoff frequency.

At frequencies below cutoff the propagation constant β becomes imaginary, thus it becomes an attenuation constant:

$$\beta = \frac{\omega\sqrt{\varepsilon_r}}{c}\sqrt{1-(f_c/f)^2} = j\frac{\omega\sqrt{\varepsilon_r}}{c}\sqrt{(f_c/f)^2-1} = j\alpha \qquad (3.4a)$$

$$\alpha = \frac{\omega\sqrt{\varepsilon_r}}{c}\sqrt{(f_c/f)^2-1} = \frac{\omega_c\sqrt{\varepsilon_r}}{c}\sqrt{1-(f/f_c)^2} \text{ Np/m} \qquad (3.4b)$$

That is, the waves in all modes attenuate exponentially hence the name Evanescent Mode Waveguide (EWG). This attenuation should not be mixed up with attenuation due to resistive loss. It is due to reflection of the waves, much such as attenuation in lossless (reactive) filter elements in their stopbands. Although in general the attenuation constant is frequency dependent, from the above equations it is seen that it becomes frequency independent for frequencies far below cutoff.

In the cutoff region the characteristic impedance becomes purely imaginary. For example the V/I based impedance becomes

$$Z_{cV,I} = \frac{V}{I} = \frac{E_{0x}b}{H_{0y}a} = \frac{b}{a}Z_w = \frac{120\pi b}{a\sqrt{\varepsilon_r}\sqrt{1-(f_c/f)^2}} = -j\frac{120\pi b}{a\sqrt{\varepsilon_r}\sqrt{(f_c/f)^2-1}} = jXo \qquad (3.5)$$

This is similar to the impedance of a lossless filter in its stopband. That is the waveguide acts as a reactive distributed element rather than a propagating transmission line. This reactive nature is exploited for realization of filters. That is, an evanescent waveguide

piece can be used in a filter such that it provides the necessary inductive coupling required. The imaginary characteristic impedance of the waveguide can be changed by varying its width and height.

Such filters can be designed in frequency ranges starting from VHF frequencies to millimeter wave frequencies, with bandwidths from 1-percent up to an octave or wider band and with wide stopbands. Actually the inductive reactances used in modeling EWG pieces are not lumped inductors. Compared to lumped inductors, they have higher rate of increase with frequency because the propagation factor β tends to zero as frequency approaches to the cutoff frequency f_c. The effect of this approximation shows itself as a shrink in bandwidth. However at frequencies well below the cutoff frequency the shrinkage in bandwidth reduces considerably.

Next section presents rigorous field theory analysis of waveguide inductive iris filter section.

3.3 Analysis of the Inductive-Iris Waveguide Filter Section

Fig 3.5a shows the filter section for analysis. For purpose of flexibility in analysis the section has been sub-divided into three components as shown in Fig 3.5b. The complete filter section, now comprises of a step junction at $z = l_1$ with a reduced waveguide in center and a reverse step at $z = l_2$. Following sections determines the scattering parameters for a filter section by virtue of combining scattering parameters obtained separately for the step junction, coupling waveguide and an inverse step junction. The approach of determining scattering parameters for each section separately provides

flexibility to the analysis, giving way to a more generalized technique that can be applied to wide variety of waveguide structures.

3.3.1 Scattering Matrix of a Step Discontinuity in the H-Plane

Fig 3.5b shows the geometry of a H-plane step. This discontinuity is a result of step change in width of the waveguide. The analysis is carried out with an assumption that only the dominant mode TE_{10} is propagating in regions I ($z < l_1$). The other modes are non propagating. Since guide II is in its evanescent mode the analysis to follow is still valid. Rigorous field theory technique proposed for E-plane filters [9] is used. For the purpose of analysis, side walls are assumed to be continuous conducting boundaries.

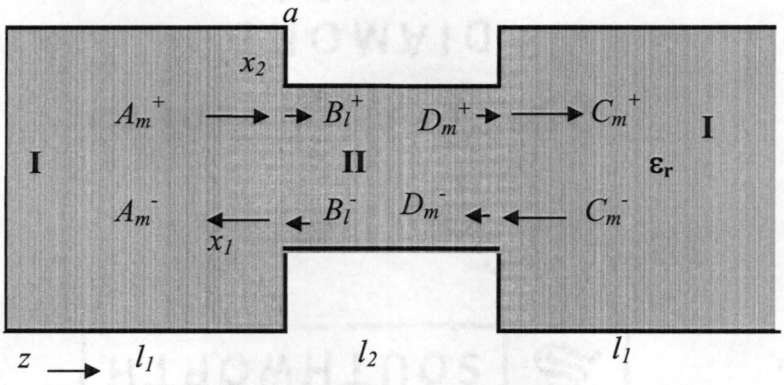

(a) Single Inductive Iris Filter Section

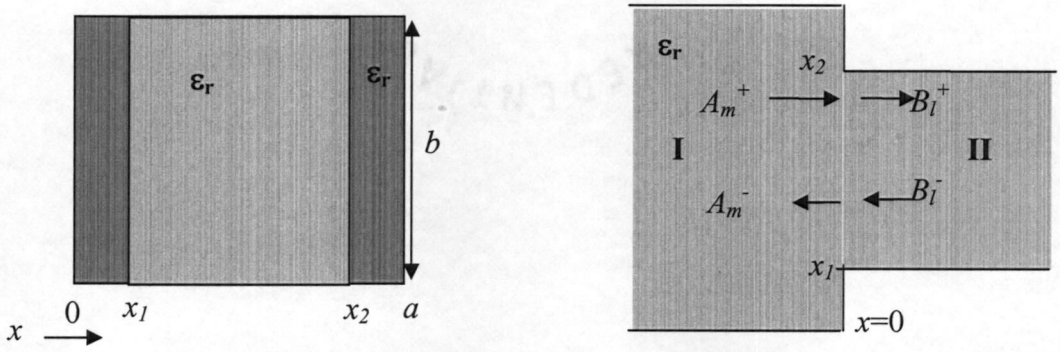

(b) Step transition from a standard waveguide to a narrower waveguide section

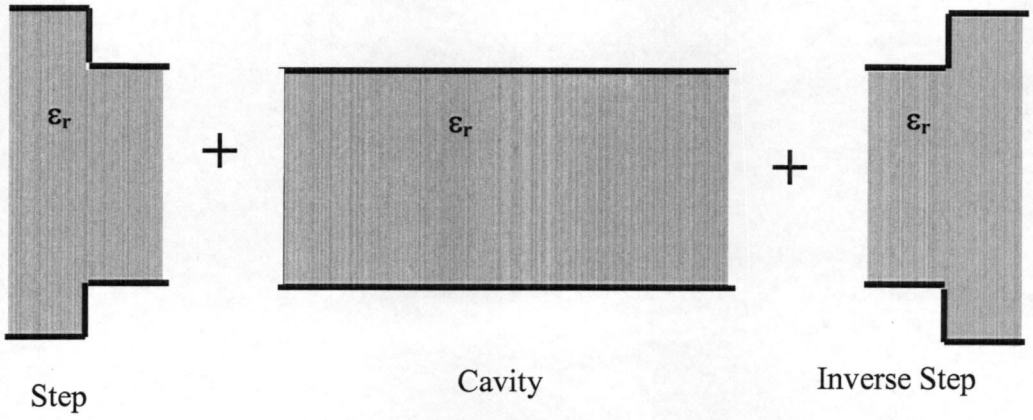

(c) Modular Approach to analyzing a Filter Section

Figure 3.5 The Proposed Filter Section (a) Single Inductive Iris Filter Section (b) Step transition from a standard waveguide to a narrower waveguide section (c) Modular Approach to analyzing a Filter Section

A.1 Definition of fields in various regions

In regions I and II, the x component of the magnetic hertzian vector potentials Φ_x is

assumed to be a sum of eigen modes. Φ_x satisfies the vector helmoltz equation and the corresponding boundary conditions and can be defined as follows

$$\Phi_x^{\ I} = \sum_{m=1}^{M} A_m^{\ I} \sin\left(\frac{m\pi x}{a}\right)\exp(-jk_{zm}^{\ I} z) \tag{3.6a}$$

$$\Phi_x^{\ II} = \sum_{l=1}^{L} B_l^{\ II} \sin\left(\frac{l\pi(x-x_1)}{x_2-x_1}\right)\exp(-jk_{zm}^{\ II} z) \tag{3.6b}$$

Using above equations the field in region I can be defined as, the y component of the electric field must be zero at x = 0 and x = a because of the presence of conducting walls.

$$E_y^{\ I} = -\omega\mu\sum_{m=1}^{\infty} k_{zm}^{\ I} A_m^{\ I} \sin\left(\frac{m\pi x}{a}\right)\exp(-jk_{zm}^{\ I} z) \tag{3.7a}$$

$$H_x^{\ I} = \sum_{m=1}^{\infty} k_{zm}^{\ I^2} A_m^{\ I} \sin\left(\frac{m\pi x}{a}\right)\exp(-jk_{zm}^{\ I} z) \tag{3.7b}$$

In region II, we have $E_y^{\ II} = 0$ at x = x_1 and at x = x_2.

$$E_y^{\ II} = -\omega\mu\sum_{l=1}^{\infty} k_{zl}^{\ II} B_l^{\ II} \sin\left(\frac{l\pi(x-x_1)}{x_2-x_1}\right)\exp(-jk_{zl}^{\ II} z) \tag{3.7c}$$

$$H_x^{\ II} = \sum_{l=1}^{\infty} k_{zl}^{\ II^2} B_l^{\ II} \sin\left(\frac{l\pi(x-x_1)}{x_2-x_1}\right)\exp(-jk_{zl}^{\ II} z) \tag{3.7d}$$

A_m^+, A_m^-, B_l^+ and B_l^- are the forward and reverse wave amplitudes in both regions as shown in Fig.3.5b and M and L represent the number of eigen modes considered in each region. The unknown coefficients, A_ms and B_ls can be determined by normalizing the power of the wave to 1 W or j W for the propagating or evanescent mode respectively as follows:

The power transported along the z direction is given by

$$W_m = \iint_S (E_m \times H_m^*) dS \tag{3.8a}$$

with $E_{ym}^{\ v}$ and $H_{xm}^{\ v}$ as the non-zero field components, v = I to II, we have

$$W_m = -\int_x \int_y (E_{ym} \times H_{xm}^*) dxdy \tag{3.8b}$$

At z = l_1 in region I

$$W_m^{\ I} = \int_{x=0}^{a} \int_{y=0}^{b} \omega\mu {k_{zm}}^{I^3} {A_m}^{I^2} \sin^2\left(\frac{m\pi x}{a}\right) dxdy \tag{3.8c}$$

equating $W_m^{\ I}$ to 1 watt or j watts as the case may be,

$$A_m^{\ I} = \sqrt{\frac{2}{\omega\mu a_1 b \,|\, k_{zm}^{\ I} \,|^3}} \tag{3.9a}$$

Similarly, evaluating powers in regions II and equating to 1 watt of j watts, we get the expression for B_l^{II} as follows:

$$B_l^{\ II} = \sqrt{\frac{2}{\omega\mu a_2 b \,|\, k_{zl}^{\ II} \,|^3}} \tag{3.9b}$$

where

$a_2 = x_2 - x_1$

k_{zm}^I and k_{zl}^{II} are the x directed wave numbers given as follows:

$${k_{zm}}^{I^2} = \omega^2 \mu_0 \varepsilon_0 \varepsilon_r - \left(\frac{m\pi}{a_1}\right)^2 \tag{3.10a}$$

$${k_{zl}}^{II^2} = \omega^2 \mu_0 \varepsilon_0 \varepsilon_r - \left(\frac{l\pi}{a_2}\right)^2 \tag{3.10b}$$

A.2 Scattering Matrix Formulation

In regions *I* and *II*, electric and magnetic fields can be expressed in terms of wave amplitudes as follows:

$$E_y^I = -\omega\mu \sum_{m=1}^{M} k_{zm}^I A_m^I \sin\left(\frac{m\pi x}{a}\right)\left(A_m^+ e^{-jk_{zm}^I z} + A_m^- e^{+jk_{zm}^I z}\right) \tag{3.11a}$$

$$H_x^I = \sum_{m=1}^{M} k_{zm}^{I^2} A_m^I \sin\left(\frac{m\pi x}{a}\right)\left(A_m^+ e^{-jk_{zm}^I z} - A_m^- e^{+jk_{zm}^I z}\right) \tag{3.11b}$$

$$E_y^{II} = -\omega\mu \sum_{l=1}^{L} k_{zl}^{II} B_l^{II} \sin\left(\frac{l\pi(x-x_1)}{x_2-x_1}\right)\left(B_l^+ e^{-jk_{zl}^{II} z} + B_l^- e^{+jk_{zl}^{II} z}\right) \tag{3.11c}$$

$$H_x^{II} = \sum_{l=1}^{L} k_{zl}^{I^2} B_l^{II} \sin\left(\frac{l\pi(x-x_1)}{x_2-x_1}\right)\left(B_l^+ e^{-jk_{zl}^{II} z} + B_l^- e^{+jk_{zl}^{II} z}\right) \tag{3.11d}$$

The fields in region I and region II are not the same because of the presence of the step discontinuity at $z = l_1$. Fields can be seen to satisfy the following boundary conditions:

$$E_y^I = E_y^{II}; (x_1 < x < x_2) \tag{3.12a}$$

$$= 0;\ (0 \le x \le x_1); (x_2 \le x \le a)$$

$$H_x^I = H_x^{II}; (x_1 < x < x_2) \tag{3.12b}$$

Thus, by matching the boundary conditions at z = l_1 for regions I and II, the multimode scattering parameter matrix at the junction can be determined.

For equating the total electrical fields on both the sides at z = 0, we add the fields on the right hand side and integrate both sides over 0 to a after multiplying by $\sin(\frac{m\pi x}{a_1})$

$$\int_0^a E_y{}^I \sin\left(\frac{m\pi x}{a_1}\right) dx = \int_0^{x_1} 0\,dx + \int_{x_1}^{x_2} E_y{}^{II} \sin\left(\frac{m\pi x}{a_1}\right) dx + \int_{x_2}^{0} 0\,dx \tag{3.13}$$

because of the orthogonal property of the trigonometric functions, except for one term, all other terms of the series on the left hand side vanish.

Equations (3.11) can be rewritten as

$$k_{zm}{}^{I} A_m{}^{I} (A_m{}^{+} + A_m{}^{-}) \frac{a_1}{2} = \sum_{l=1}^{L} k_{zl}{}^{II} B_l{}^{II} (B_l{}^{+} + B_l{}^{-}) H_{ml} \qquad (3.14)$$

where H_{ml} is given as follows:

$$H(m,l) = \int_{x_1}^{x_2} \sin(\frac{m\pi}{a_1} x) \sin(\frac{l\pi(x - x_1)}{a_2}) dx \qquad (3.15)$$

Equation can be written as:

$$(F_E)[A_m{}^{+} + A_m{}^{-}] = (Y_E)[B_l{}^{+} + B_l{}^{-}] \qquad (3.16)$$

where

$$(F_E)_{ml} = \frac{k_{zm}{}^{I} A_m{}^{I} a_1}{2} \qquad (3.17a)$$

$$(Y_E)_{ml} = k_{zl}{}^{II} B_l{}^{II} hm(m,l) \qquad (3.17b)$$

Multiplying both sides of (3.16) by $(F_E)^{-1}$

$$[A_m{}^{+} + A_m{}^{-}] = (L)[B_l{}^{+} + B_l{}^{-}] \qquad (3.18)$$

where

$$(L) = (F_E)^{-1} (Y_E) \qquad (3.19)$$

We have another boundary condition at z = 0 as given in (3.12b)

Since H_x is discontinuous at the interface because of the presence of conducting walls, we can not equate the fields on the right hand side and then equate $H_x{}^{I}$.

Multiplying both sides by the orthogonal function corresponding to region II, i.e. $\sin(\frac{l\pi(x - x_1)}{x_2 - x_1})$ we can obtain the following equation:

$$\sum_{m=1}^{M} K_{zm}{}^{I^2} A_m{}^{I} H_{ml} (A_m{}^{+} - A_m{}^{-}) = K_{zl}{}^{II^2} B_l{}^{II} \frac{x_2 - x_1}{2} (B_l{}^{+} - B_l{}^{-}) \qquad (3.20)$$

The above equation can be rewritten as

$$\sum_{m=1}^{M}(F_H)[A_m^+ - A_m^-] = (Y_H)[B_l^+ - B_l^-] \quad (3.21)$$

$$(F_H)_{ml} = (k_{zm}{}^{I})^2 A_m{}^{I} hm(m,l) \quad (3.22a)$$

$$(Y_H)_{mm} = \frac{a_2 (k_{zl}{}^{II})^2 B_l^{II}}{2} \quad (3.22b)$$

Let $(Z) = (Y_H)^{-1}(F_H)$

The above equation can be reduced to

$$(Z)[(A_m^+) - (A_m^-)] = [(B_l^+) - (B_l^-)] \quad (3.23)$$

Now, we have the final matrix equations for the junction at z = 0 as

$$[A_m^+ + A_m^-] = (L)[B_l^+ + B_l^-] \quad (3.18)$$

$$(Z)[(A_m^+) - (A_m^-)] = [(B_l^+) - (B_l^-)] \quad (3.23)$$

Premultiply eq(3.23) by (L)

We get,

$$(L)(Z)[(A_m^+) - (A_m^-)] = (L)[(B_l^+) - (B_l^-)] \quad (3.24)$$

subtracting (3.24) from (3.18), we get

$$(A_m^-) = ([(L)(Z) + (I)]^{-1} \times [(L)(Z) - (I)])(A_m^+) + ([(L)(Z) + (I)]^{-1} \times (L))(B_l^-) \quad (3.25)$$

The above equation corresponds to

$$(A_m^-) = (S_{11})(A_m^+) + (S_{12})(B_l^-) \quad (3.26)$$

where,

$$(S_{11}) = [(L)(Z) + (I)]^{-1} \times [(L)(Z) - (I)] \quad (3.27a)$$

$$(S_{12}) = [(L)(Z) + (I)]^{-1} \times (L) \quad (3.27b)$$

Substituting from eq (3.26) into (3.18), we can obtain (S_{22}) by rearranging the equation

in form of

$$(B_l^+) = (S_{21})(A_m^+) + (S_{22})(B_l^-) \tag{3.28}$$

$$(S_{22}) = (I) - 2 \times (Z) \times [(L)(Z) + (I)]^{-1} \times (L) - (I) \tag{3.29a}$$

$$(S_{21}) = (S_{12}) \tag{3.29b}$$

3.3.2 Scattering Parameters for the inverse step

The exact procedure as discussed above can be used to determine S parameters for the step shown in Fig. 3.5b. Another method to obtain S parameters is by using the following transformations to the S matrix determined above

$$\begin{aligned} (S_{11})_{lm} &= (S_{22})_{ml} \\ (S_{12})_{lm} &= (S_{21})_{ml} \\ (S_{21})_{lm} &= (S_{12})_{ml} \\ (S_{22})_{lm} &= (S_{11})_{ml} \end{aligned} \tag{3.30}$$

3.3.3 Scattering Parameters for the Cavity

A rectangular cavity can be analyzed as shown in Fig. 3.6. P_m^+, P_m^-, Q_n^+ and Q_n^- are the incident and reflected wave amplitudes at the input and output respectively. A transmission line of length l induces a phase lag of $\exp(-jk_{zm}l)$ when traveling from left to right. Where k_{zm} is the x directed wave number and is calculated as

$$k_{zm}^{\ 2} = \omega^2 \mu_0 \varepsilon_0 \varepsilon_r - \left(\frac{m\pi}{a_1}\right)^2 \tag{3.31}$$

where a_1 is the width of the waveguide. Thus the wave amplitudes can be correlated as

$$Q_n^+ = \exp(-jk_{zm}l) P_m^+ \tag{3.32a}$$

and

$$P_m^- = \exp(+jk_{zm}l)Q_n^- \tag{3.32b}$$

thus the S parameter can be obtained from (3.32a) and (3.32b) as

$$[S_{11}]_{mn} = 0 \tag{3.33a}$$

$$[S_{22}]_{mn} = 0 \tag{3.33b}$$

$$[S_{12}]_{mn} = \begin{bmatrix} 0 & if\ m \neq n \\ \exp(-jk_{zm}l)\, if\ m = n \end{bmatrix} \tag{3.33c}$$

$$[S_{21}]_{mn} = \begin{bmatrix} 0 & if\ m \neq n \\ \exp(+jk_{zm}l)\, if\ m = n \end{bmatrix} \tag{3.33d}$$

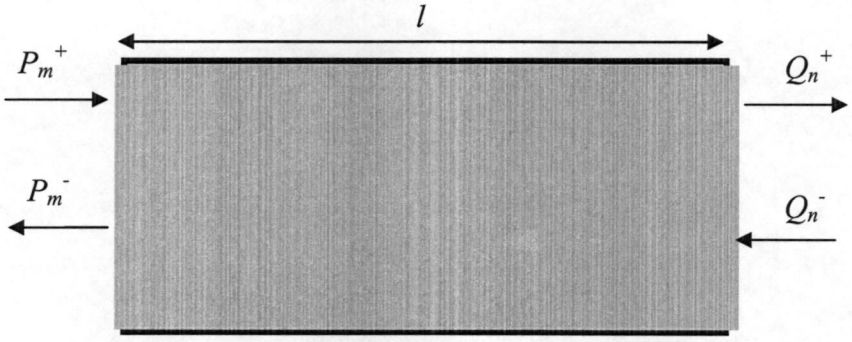

Figure 3.6 A dielectric loaded rectangular waveguide

3.3.4 Scattering Matrix for the filter section

Scattering matrix for the complete filter is obtained by combining the scattering matrices for each section sequentially going left to right. Fig. 3.7 shows the algorithm to obtain the scattering matrix of the filter section by suitable combination of the individual scattering matrices.

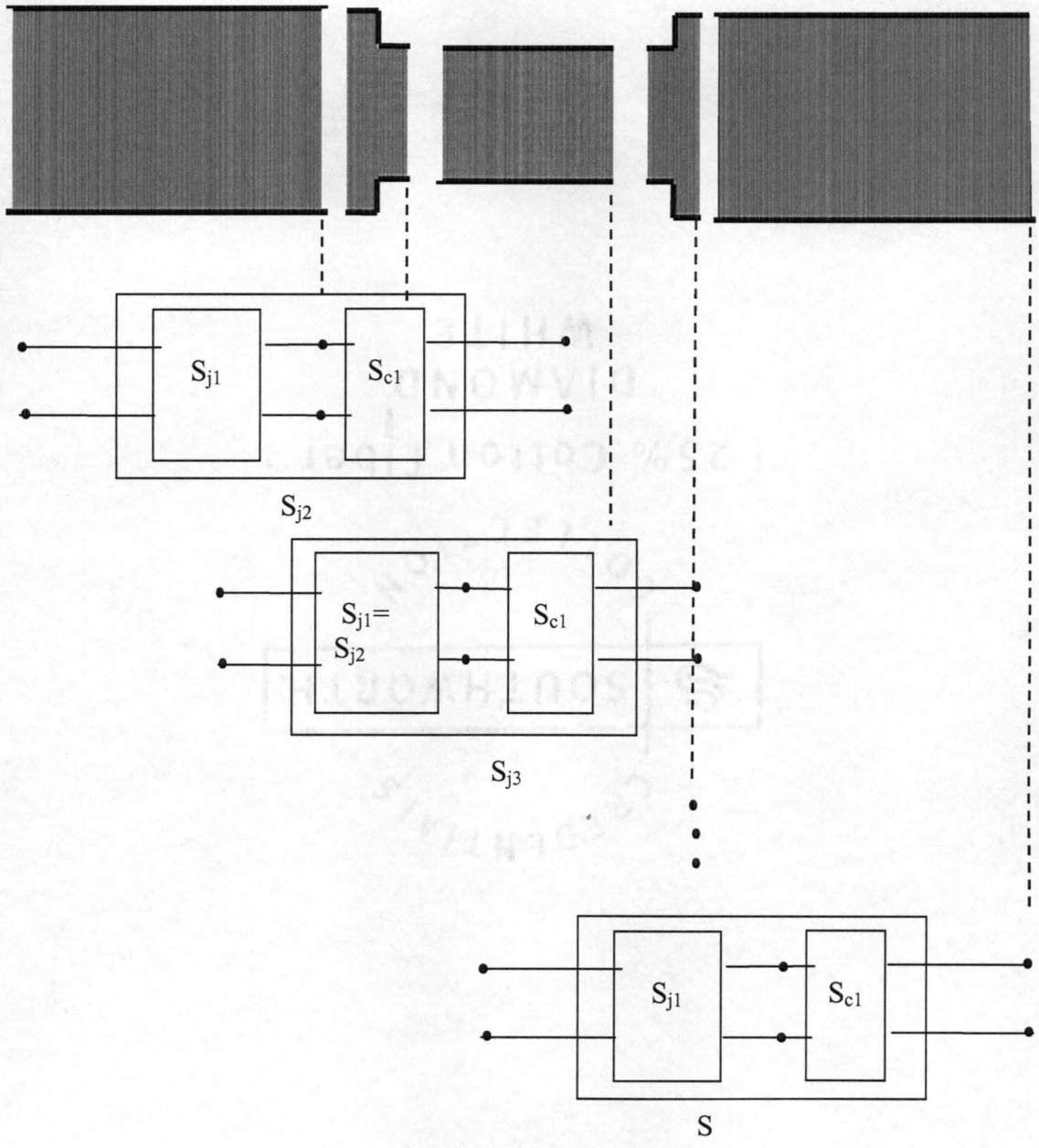

Figure 3.7 Block Diagram showing the algorithm to obtain the overall scattering matrix of the filter section. The technique can be extended to obtain the overall scattering matrix for the entire filter.

The scattering matrix of the first coupling section is combined with the former (S_j) into (S_{j+1}) which has the following submatrices:

$$S_{j2(11)} = S_{j1(11)} + S_{j1(12)} \bullet (E - S_{c1(11)} \bullet S_{j1(22)})^{-1} \bullet S_{c1(11)} \bullet S_{j1(21)} \quad (3.34a)$$

$$S_{j2(12)} = S_{j1(12)} \bullet (E - S_{c1(11)} \bullet S_{j1(22)})^{-1} \bullet S_{c1(12)} \quad (3.34b)$$

$$S_{j2(21)} = S_{c1(21)} \bullet (E - S_{j1(22)} \bullet S_{c1(11)})^{-1} \bullet S_{j1(21)} \quad (3.34c)$$

$$S_{j2(22)} = S_{c1(22)} + S_{c1(21)} \bullet (E - S_{j1(22)} \bullet S_{c1(11)})^{-1} \bullet S_{j1(22)} \bullet S_{c1(12)} \quad (3.34d)$$

where E denotes m x m the unity matrix.

The proposed filter section can also be analyzed using the exact same field theory analysis, without disintegrating the filter section in step, waveguide, step sequence. The modular approach discussed above is limited in its application as it fails to predict accurately the higher mode interactions for smaller waveguide lengths of the order of few hundred microns.

3.4 Filter Design

The filters has been designed using the impedance (K-) inverter approach as discussed in 2.5c is used. The K values are obtained from the prototype discussed in 2.2. An iterative design process is adopted for design of every section. Scattering matrix of each filter section is obtained by assuming lengths for the half resonator section and the coupling section. From the scattering matrix obtained, the impedance inverter parameter K, and the effective electrical delay, ϕ are determined using eq (3.35). Considering Fig. 1e as the equivalent circuit representation of the filter section, the impedance inverter parameter, K and the effective electrical delay, ϕ can be expressed in terms of the series (X_a) and shunt (X_b) reactances as,

$$K = \left|\tan\left(\phi/2 + \tan^{-1}(X_a)\right)\right| \tag{3.35a}$$

$$\phi = -\tan^{-1}(2X_b + X_a) - \tan^{-1}(X_a) \tag{3.35b}$$

For a given set of physical dimensions, X_a and X_b can be extracted from the multi-mode S-parameters of the filter section as determine in section 3.3 from the following equations:

$$X_b = \frac{2S_{21}(1,1)}{(1-S_{11}(1,1))^2 - S_{21}(1,1)^2} \tag{3.36a}$$

$$X_a = \frac{1+S_{11}(1,1)-S_{21}(1,1)}{1-S_{11}(1,1)+S_{21}(1,1)} \tag{3.36b}$$

For an N-resonator bandpass filter design, l_1 and l_2 for each of the N+1 sections can be calculated by matching the K value for each section to the desired value of K obtained from the lowpass filter prototype values [34], and equating ϕ to be equal to 90° at the center frequency.

The K value obtained from eq. 3.35 and 3.36 reflect the lengths of individual filter elements. Thus lengths being a variable can be iterated to obtain desired value of K and ϕ with the following optimization function:

$$F_{optimization} = abs(\phi - \frac{\pi}{2}) + abs(K - K_{desired}) \tag{3.37}$$

To obtain, ϕ equal to 90° and K equal to the prototype value a code has been implemented in Matlab using the optimization tool box. The process is highly efficient and can predict accurate section lengths with very few length iterations.

It can be seen that the proposed technique offers some distinct advantages over the conventional design procedures. With less number of iterative variables, three for every filter section, as compared to the conventional design techniques, the new approach

provides more flexibility. The approach can be used to realize complex filter configurations with higher number of resonators as the synthesis complexity is independent of number of resonators. Whereas in the conventional techniques, synthesis becomes complex with increase in number of resonators as the number of iterative variables is increased. It is difficult to preserve the shape of response while designing filters using conventional techniques which result in highly length sensitive filters. The new approach preserves the filter response as every filter section satisfies ϕ equal to 90° and has K value equal to the desired coupling coefficient at the center frequency. It should be noted that with an increase in number of resonators the synthesis time increase linearly as opposed to a nonlinear increase in synthesis time using conventional design procedures.

3.5. Results and Validation

The analysis technique discussed above is unique in its ability to consider interactions among higher order modes accurately. As can be expected, an increase in number of modes i.e. M and L, will lead to longer computing times. Table 2 shows change in element lengths for a third order filter. Fig. 3.8a - 3.8c show convergence as seen in element length with an increase in number of modes. Use of 50 modes should be sufficient in synthesis and analysis of filters discussed later.

Table 2 Element lengths for a N = 3 bandpass filter
(Freq= 29GHz, $\Delta = 0.03$, Ripple = 0 dB, $\varepsilon_r = 2.22$, $a_1 = 5$mm, $a_2 = a_3 = 2.5$ mm)

Modes.	l_1 (mm)	l_2 (mm)	l_3 (mm)	l_4 (mm)
10	0.756	3.696	2.917	3.719
25	0.724	3.719	2.883	3.740
40	0.720	3.720	2.880	3.743
50	0.719	3.722	2.879	3.744
60	0.719	3.722	2.879	3.744

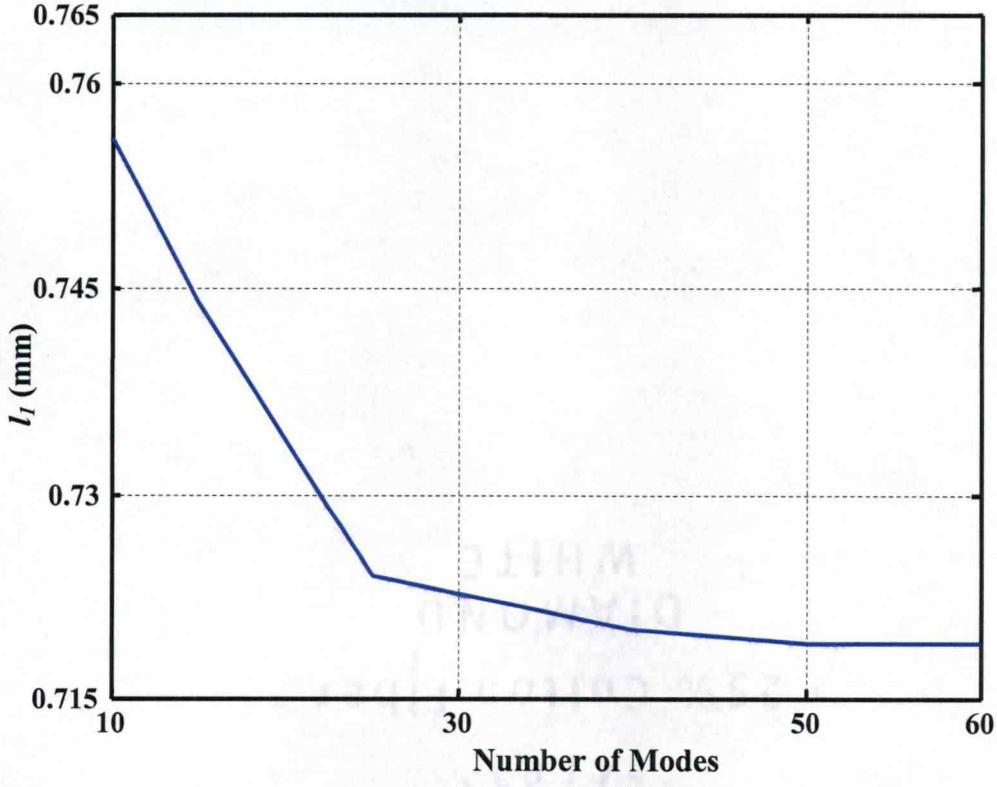

(a) Convergence in length of inductive coupler for first filter section

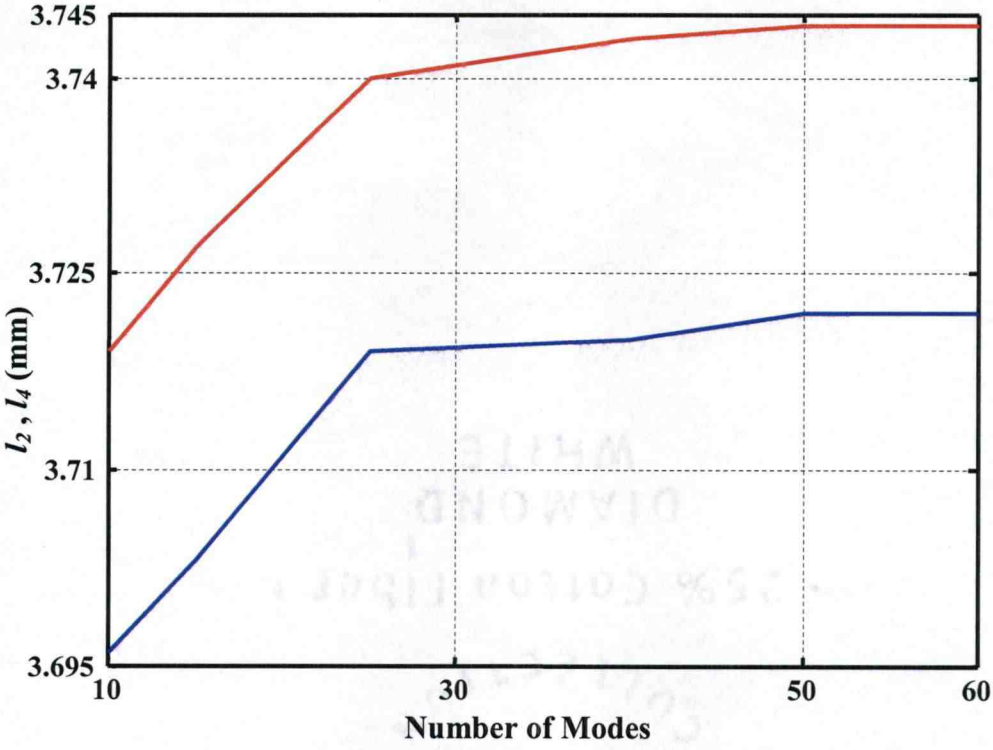

(b) Convergence in length of resonators for first and second filter section

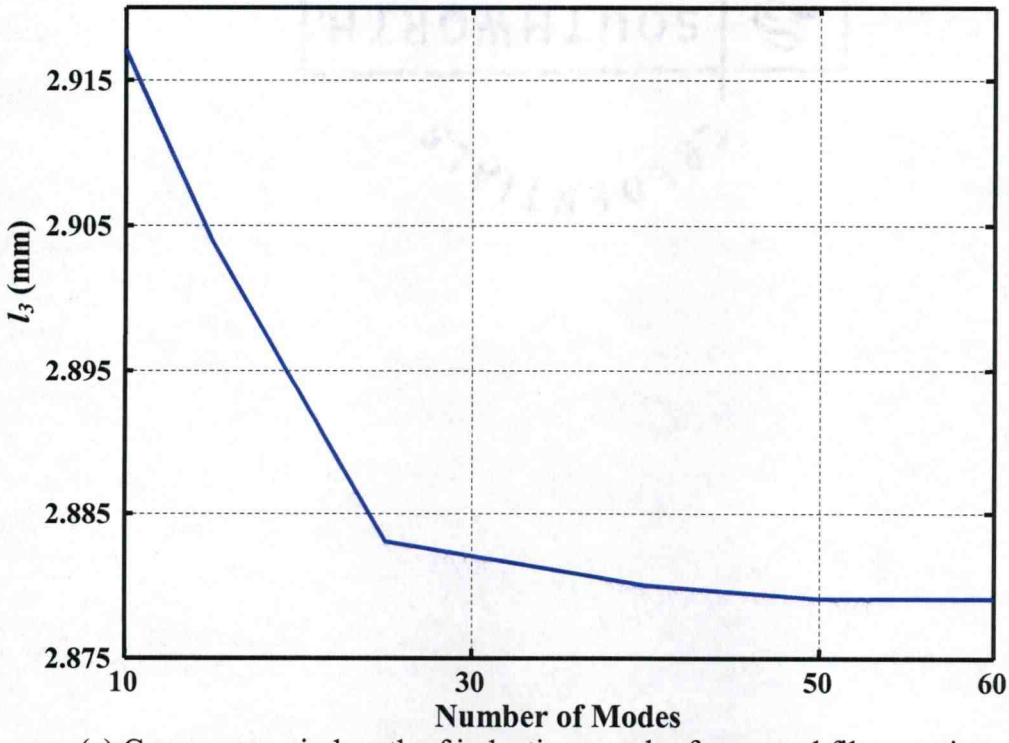

(c) Convergence in length of inductive coupler for second filter section

Figure 3.8 Convergence observed for element lengths with increasing number of modes

Initially, to validate the current theory, we simulated the 3-resonator iris waveguide filter reported in [27]. Total number of modes, M=L=40 turned out to be sufficient. Fig. 3.9 shows the theoretical response in comparison with the reported results. It may be seen that both results match very well.

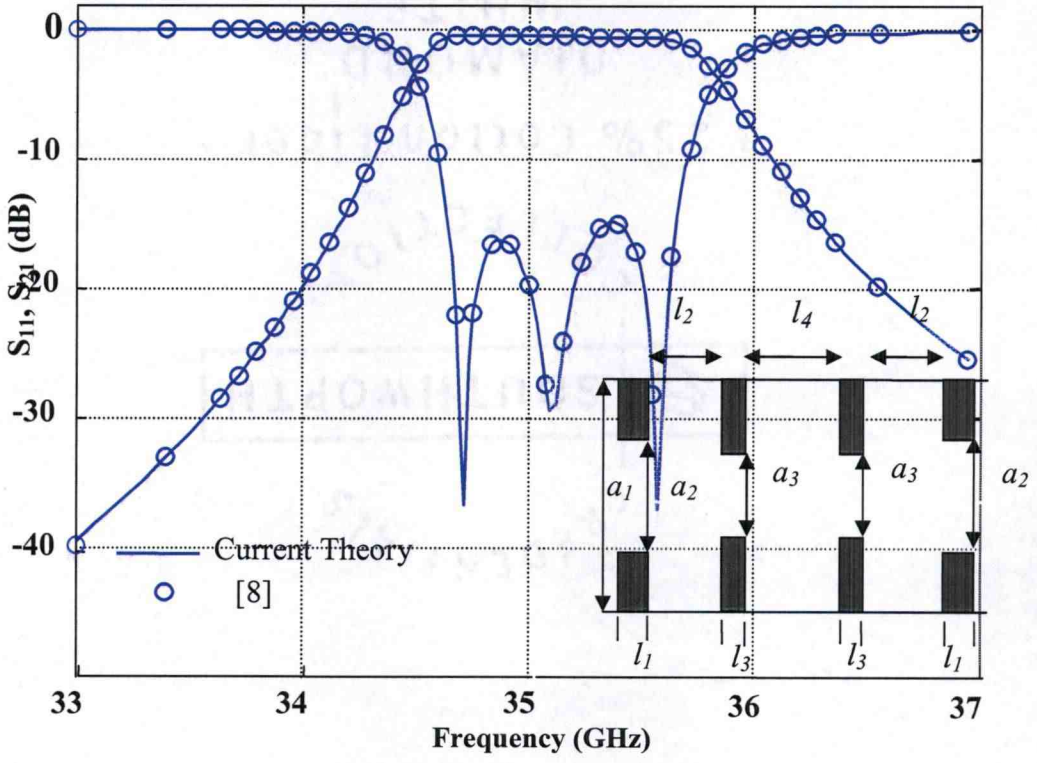

Figure 3.9 Simulated Response for empty waveguide Inductive Iris filter reported in [8]. a_1 = 7.1mm, a_2 = 3.6mm, a_3 = 2.4mm, b = 3.55mm, l_1 = 1.45mm, l_2 = 4.15mm, l_3 =1.1mm, l_4 =4.7 mm

Next, to demonstrate the feasibility of via-implementation, a filter section with dimensions as shown in Fig. 3.10 was considered (corresponding to the second section of a Maximally flat design, fractional bandwidth, Δ=0.03, f_o= 29 GHz, with K and ϕ values of 0.0333 and 90° respectively). Fig. 3.10 shows the variation of filter design parameters, K and ϕ as a function of via-separation d. The diameter of via is 150 μm. The filter section was analyzed in a 3D full-wave EM simulator [33]. It may be seen that for via separations up to 250 μm, both K and ϕ show negligible change compared to the conventional dielectric filled rectangular waveguide with continuous conducting side walls, demonstrating that via-implementation does not affect the performance for smaller separations.

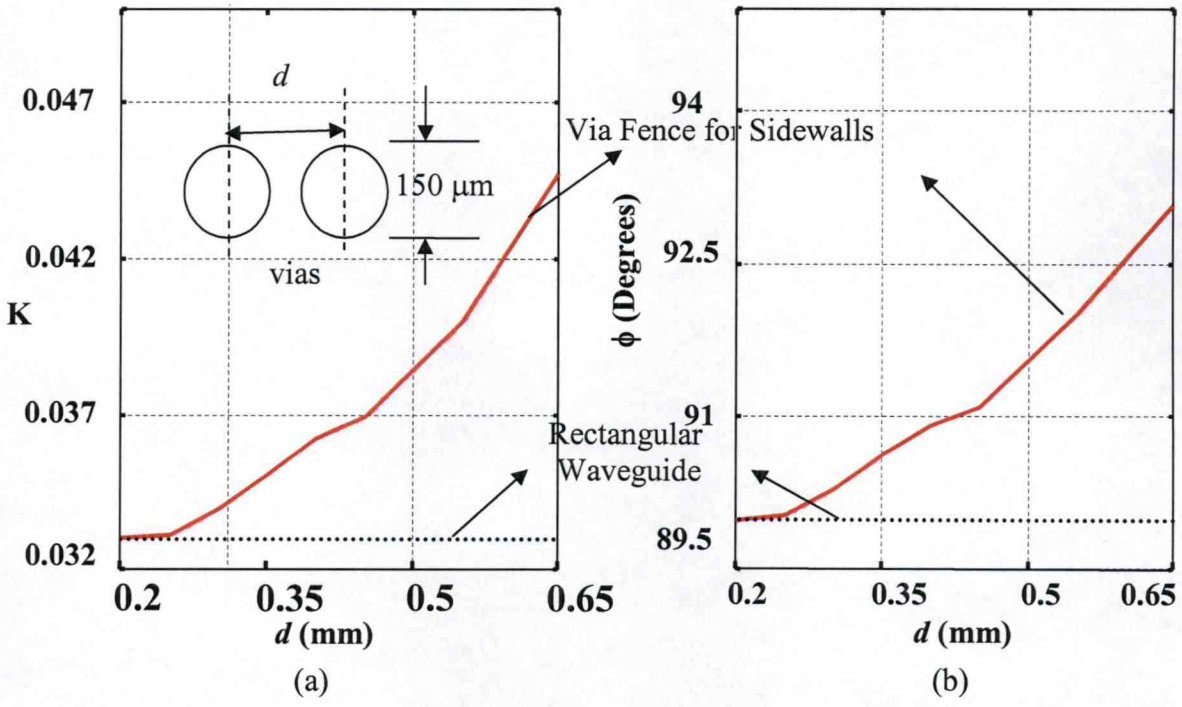

Figure 3.10 K and ϕ variation for structure in Fig. 3.5a (side walls replaced by vias) [38] a = 5 mm, b=3.556 mm, l_1 = 1.872 mm, l_2 = 2.879 mm, x_2-x_1 = 2.5 mm, f_o=29 GHz

To demonstrate the versatility of the proposed analysis and synthesis technique, three filters have been designed in the Ka, Ku and X-bands. Specifications and dimensions for the designed filters are given in Table 3. Figs. 3.11a, 3.11c, 3.11e show the theoretical response of the filters superposed with the response obtained from HFSS [33]. Series of via is realized using a via diameter of 150 μm and pitch of 250 μm. It may be seen that the frequency response matches well for all three filter designs.

Table 3 Via-only bandpass filters in Ka, Ku and X bands [38]

No.	Filter Specs. (Three resonators)	Section lengths (*mm*)	Total Filter length *(mm)*	b *(mm)*	Section Width (*mm*)
A.	f_o=29 GHz, Δ = 0.03, ε_r = 2.22 (Rogers RT Duroid), Maximally Flat	l_1 = 0.719 l_2 = 3.722 l_3 = 2.879 l_4 = 3.744	18.386	3.556	a_1 = 5.0 a_2 = 2.5 a_3 = 2.5
B.	f_o=14 GHz, Δ = 0.05, ε_r = 7.015(Dupont 943 green tape) Chebyshev Ripple= 0.05dB	l_1 = 1.565 l_2 = 3.936 l_3 = 2.445 l_4 = 4.298	20.189	3.15	a_1 = 5.75 a_2 = 3.5 a_3 = 3.0
C.	Freq = 10 GHz, Δ = 0.05, ε_r =7.015 (Dupont 943 green tape) Chebyshev Ripple =0.05dB	l_1 =2.555 l_2 =5.535 l_3 =2.292 l_4 =6.439	27.205	3.15	a_1 = 8.5 a_2 = 5.0 a_3 = 3.5

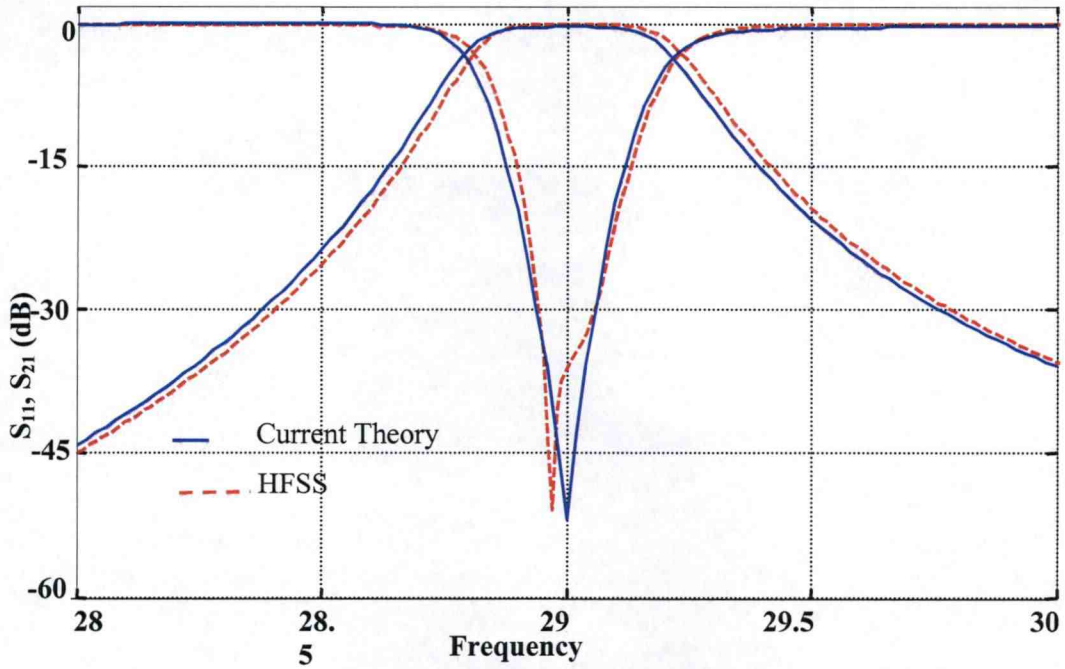

(a) Frequency Response for Design A, Table 3

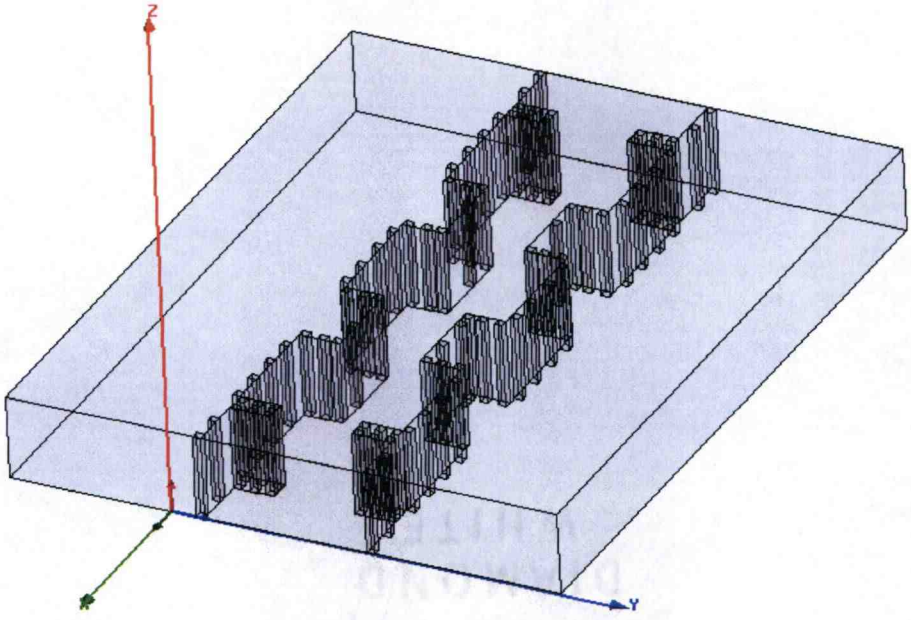

(b) 3D model of Design A as simulated in HFSS

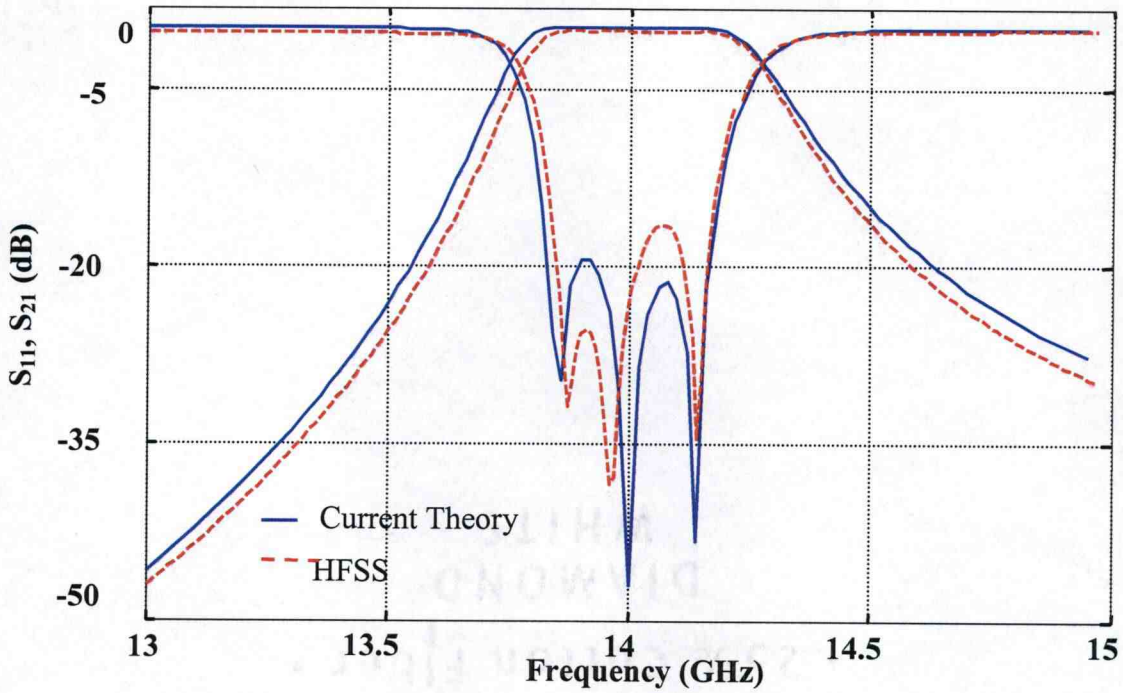

(b) Frequency Response for Design B, Table 3

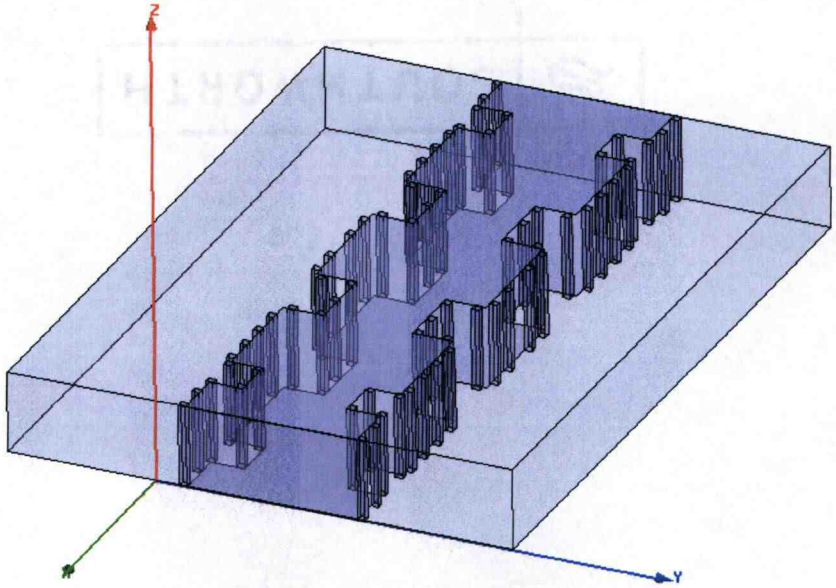

(d) 3D model of Design B as simulated in HFSS

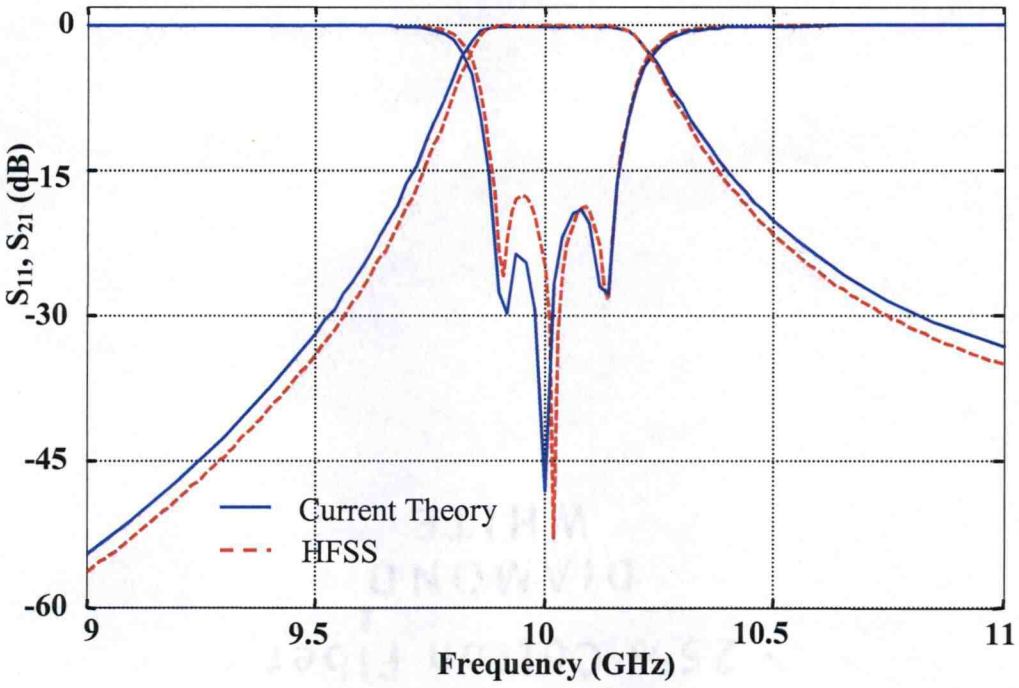

(c) Frequency Response for Design C, Table 3

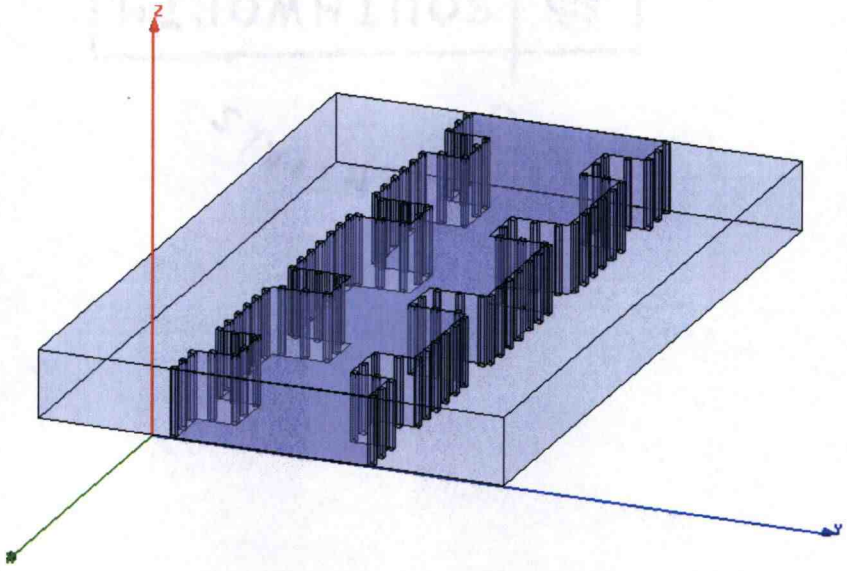

(f) 3D model of Design C as simulated in HFSS

Figure 3.11 Response for via-only filters given in Table 3.

Fig. 3.12 shows a footprint comparison for the three filters designed in table 3. As expected the length of filters is small, due to the fact that the filters are uniformly filled with dielectric. Dielectric filled waveguides, have reduced broadwall dimensions by a factor of $\sqrt{\varepsilon_r}$, thus leading to lower cutoff frequency and smaller wavelengths as compared to a empty waveguide.

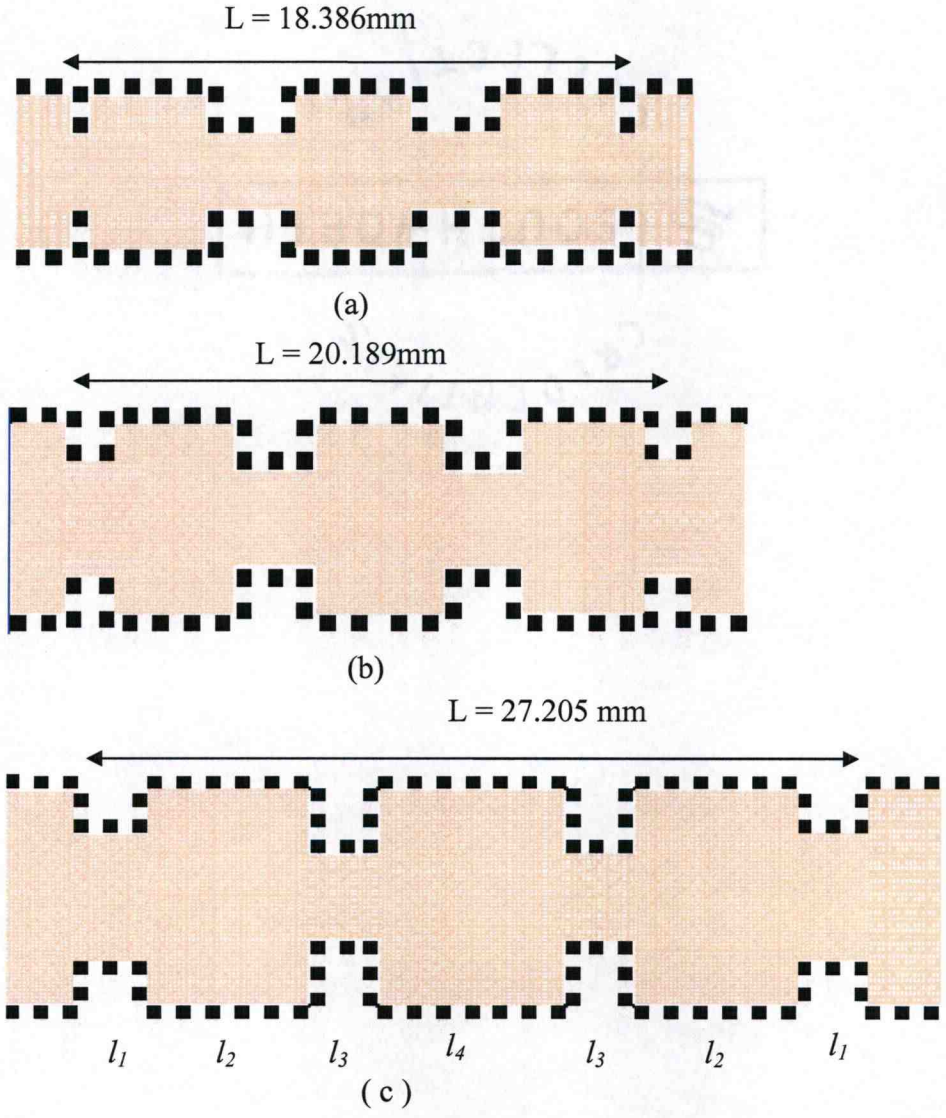

Figure 3.12 Footprint comparisons for filters from Table 2.

Fig. 3.13 shows the performance of filter designed at center frequency of 14GHz (Design B) in Table 3 when the perfect E boundaries in HFSS are replaced with copper conductors. Perfect E boundary in HFSS is used to emulate an ideal metallic surface. Thus, it becomes necessary to simulate the proposed filters with the use of conductors such copper or silver. It can be seen that the simulated response gives a close match to the obtained theoretical response from Matlab.

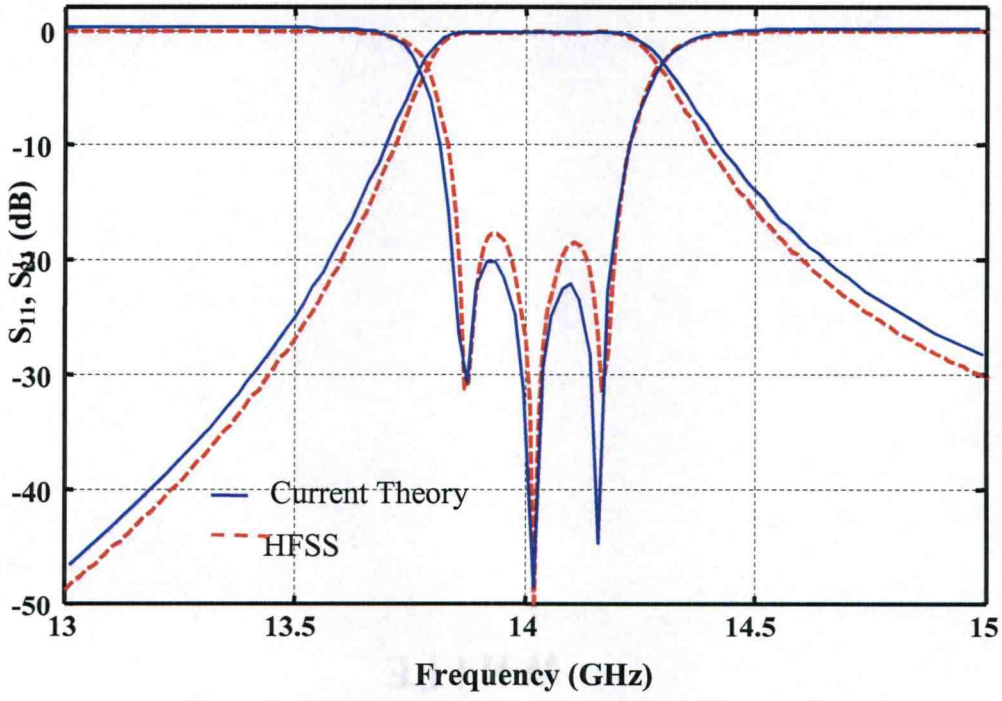

Figure 3.13 Frequency response for filter design B from Table 3.

3.5.1 Sensitivity Analysis

Sensitivity analysis has been carried out to look at the effect of change in filter dimensions on the frequency response. This is important because LTCC substrates offer wide variation in physical dimensions, as it is offered to heat treatment. To consider the shrinkage and expansion effects, the designed filters have been simulated for change in dimensions of ±5%.

Fig. 3.14 shows change in transmission coefficient (S_{21}) with change in dimension along the x axis i.e. the length of the filter. It is assumed that there is no change in filter dimensions along the y and z axis. The width and height of waveguide elements can be obtained from design B reported in Table 3. Table 4 gives the length of filter sections for which the frequency response is shown in Fig. 3.14.

Table 4. Modified lengths for Design B reported in Table 3.

Design	% shrinkage	l_1 (mm)	l_2 (mm)	l_3 (mm)	l_4 (mm)
A	0	1.565	3.936	2.445	4.298
B	1.25	1.545	3.887	2.414	4.244
C	2.50	1.526	3.838	2.384	4.191
D	3.75	1.506	3.788	2.353	4.137
E	5.0	1.487	3.739	2.322	4.083

It can be seen from Fig. 3.14 that if all the lengths are scaled uniformly there is a uniform shift in center frequency of the filter.

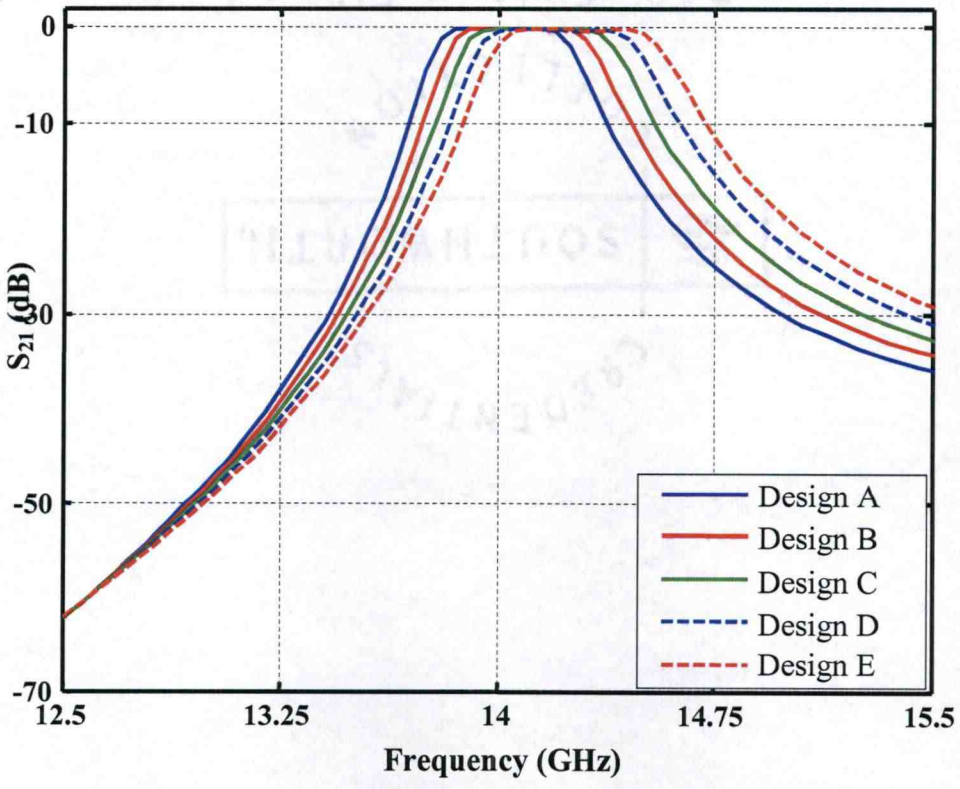

Figure 3.14 Effect on S_{21} with change in length of the filter reported in Table 3.

Fig. 3.15 shows change in S_{21} for shrinkage along the y axis i.e. the width of the waveguide elements. It is assumed that there is no change along the x and z axis. Table 5 gives the modified widths for Fig. 3.15.

Table 5 Modified widths for design B reported in Table 3.

Design	% Shrinkage	a_1 (mm)	A_2 (mm)	a_3 (mm)
A	0	5.75	3.5	3
B	0.75	5.707	3.474	2.976
C	1.5	5.664	3.447	2.954
D	2.25	5.621	3.421	2.931
E	3.0	5.577	3.395	2.909

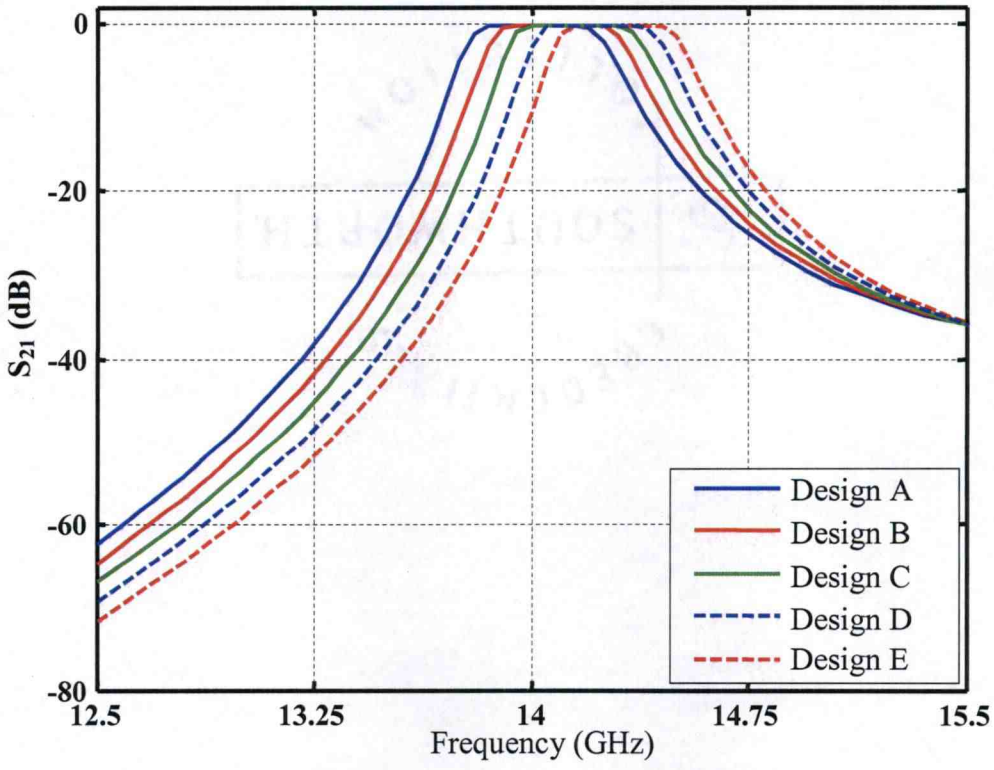

Figure 3.15 Effect on S_{21} with change in length of the filter reported in Table 3.

It can be seen from Fig. 3.15 that if all the widths are scaled uniformly there is a uniform shift in center frequency of the filter.

Fig. 3.16 shows the effect of change in S_{21} with change in height of the waveguides (z axis). Table 6 shows the shrinkage in height.

Table 6 Modified lengths for Design B reported in Table 3.

Design	% Shrinkage	*b* (mm)
A	0	3.15
B	1.25	3.111
C	2.5	3.071
D	3.75	3.032
E	5	2.992

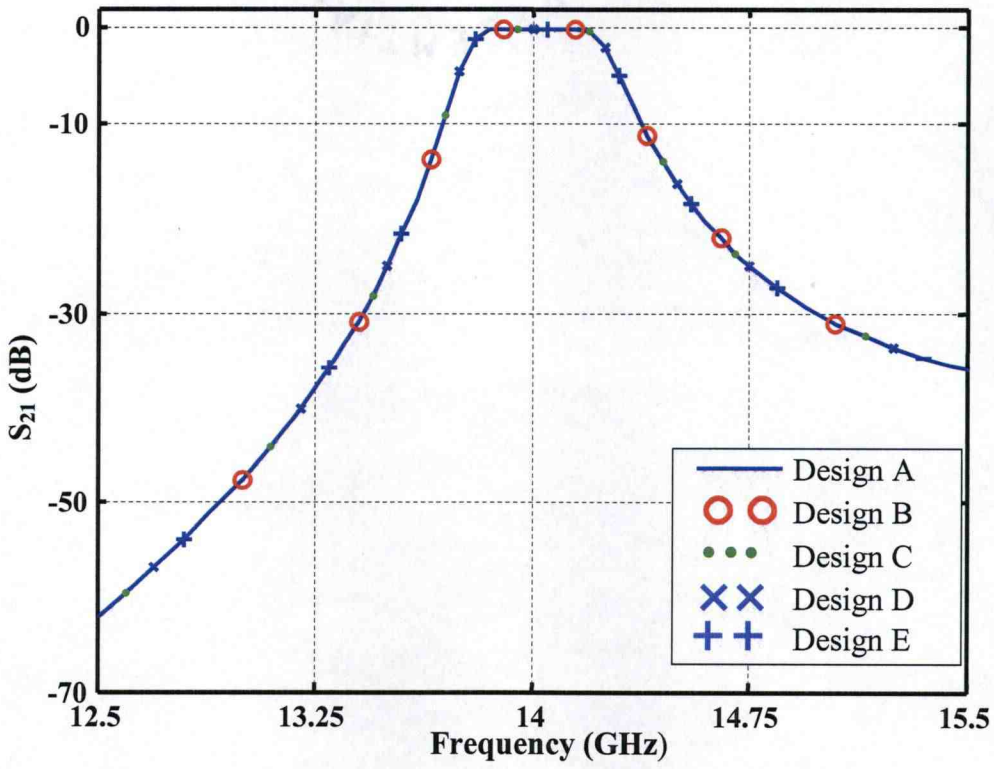

Figure 3.16 Effect on S_{21} with change in height of the filter reported in Table 3.

It can be seen that there is no change in filter response with change in height of the waveguide.

Fig. 3.17 shows the change in S_{21} when dimensions along all x, y and z are shrunk with the same percentage. Table 7 shows the modified dimensions for plot shown in Fig. 3.17

Table 7 Modified dimensions for Design B in Table 3

No.	% Shrinkage	Section lengths (*mm*)	b *(mm)*	Section Width (*mm*)
A	0	$l_1 = 1.565$	3.15	$a_1 = 5.75$
		$l_2 = 3.936$		$a_2 = 3.5$
		$l_3 = 2.445$		$a_3 = 3.0$
		$l_4 = 4.298$		
B	1.25	$l_1 = 1.545$	3.111	$a_1 = 5.678$
		$l_2 = 3.887$		$a_2 = 3.456$
		$l_3 = 2.414$		$a_3 = 2.962$
		$l_4 = 4.244$		
C	2.5	$l_1 = 1.526$	3.071	$a_1 = 5.606$
		$l_2 = 3.838$		$a_2 = 3.412$
		$l_3 = 2.384$		$a_3 = 2.925$
		$l_4 = 4.191$		
D	3.75	$l_1 = 1.506$	3.032	$a_1 = 5.534$
		$l_2 = 3.788$		$a_2 = 3.369$
		$l_3 = 2.353$		$a_3 = 2.887$
		$l_4 = 4.137$		
E	5	$l_1 = 1.487$	3.92	$a_1 = 5.462$
		$l_2 = 3.739$		$a_2 = 3.325$
		$l_3 = 2.322$		$a_3 = 2.85$
		$l_4 = 4.083$		

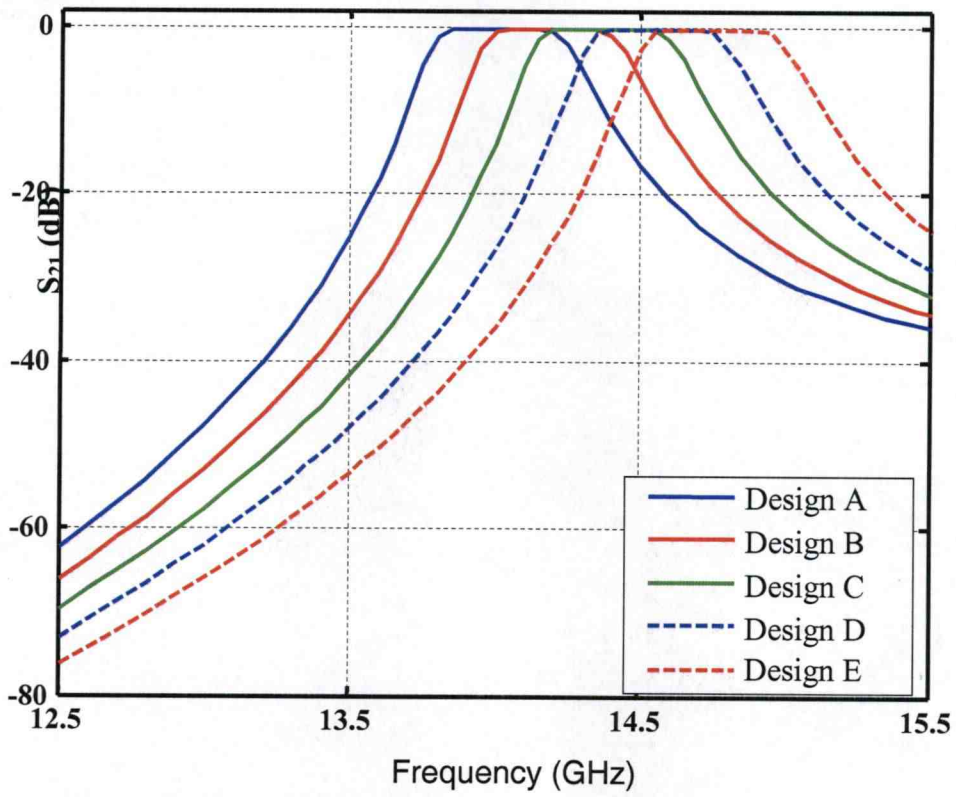

Figure 3.17 Effect on S_{21} with change in widths of filter section for Design B, Table 3.

Fig. 3.14 – 3.17 show the sensitivity analysis for Ku band. Fig. 3.14 shows that the change in length does not significantly affect the filter response. For a 5% shrinkage in length there is a shift of 300 MHz in center frequency. Change in width has a similar affect on frequency response with the center frequency been shifted by 300 MHz. These phenomena can be related to change in length of half resonator sections, which imply that as initially designed the length does not satisfy the condition of $\phi = 90°$. Fig. 3.17 shows that if all dimensions of the filter are subjected to a uniform shrinkage there is a larger shift in center frequency though the filter response is preserved. To achieve filter designs which perform efficiently even after considering shrinkage, a length correction for

individual elements can be applied at the synthesis step of filter design.

The sensitivity analysis has been carried out with higher tolerances as opposed to commonly encountered in fabrication processes. This clearly signifies the accuracy of the synthesis technique and offers it application to wide topologies for waveguide based filters.

4. VIA-ONLY E-PLANE BANDPASS FILTERS WITH SUPERIOR STOPBAND CHARACTERISTICS

Evanescent-mode filters are constructed from resonators within a below cutoff waveguide section and rectangular waveguide discontinuities for connection to standard-size input/output guides. The resonators are formed by introducing appropriate obstacles such as capacitive screws, round posts, dielectric blocks, ridges or E-plane fins [22]. In this chapter, various via-only based filter topologies with E-plane fins have been realized for LTCC applications. These filter configurations can exhibit improved stopband attenuation, which can be adjusted by varying the physical parameters. Several topologies for rectangular waveguide based E-plane Fin-line and Metal insert filters have been reported earlier. [23]-[25] . The biggest challenge with these topologies is to align the metal inserts in the waveguide cavities. This chapter puts forward compact designs for double fin-line metal insert filters in complete dielectric loaded cavities. Physical realization of these filters with conventional rectangular waveguides might be a challenge, with respect to dielectric loading of the cavities and aligning the metal inserts accurately inside. The via-only bandpass filter configurations proposed in the previous chapter, can be extended to metal insert filters, with the metal inserts being realized with via fences. The challenges with this approach can be the effect of discontinuous fins i.e. the metal inserts on the filter response. An overview of E-plane filters, with respect to accomplished techniques, their performance in the passband and stopband has been summarized below. To design E-plane bandpass filters with improved stopband performance. Several different solutions have been proposed.

1) Use of thick metal insert to reduce distance between the waveguide sidewalls and the metal insert [26] or use multiple metal inserts rather than a single one. The first one achieves good stopband performance, but has higher passband insertion loss. The second solution achieves good stopband performance but the effort required to precisely mount the metal inserts is more.

2) Use narrower or wider waveguide for the filter section depending on the position of the filter passband within the waveguide single-mode bandwidth. If the waveguide section is made narrow a significant improvement is observed in the stopband attenuation provided filter is designed at high end of the band. Increasing the waveguide housing improves the stopband performance but when filter is designed at lower end of the band.

3) Use resonators of different cutoff frequencies. This is achieved by employing sections of rectangular waveguide in which all the waveguide sections are resonant at the same fundamental frequency. However, due to different guide wavelengths in the different sections, the sections are not all simultaneously resonant at any higher frequency, resulting in an improved stopband attenuation.

4.1 Filter section

A typical filter section for fin-line E-plane waveguide filters is shown in Fig 4.1. It consists of two half resonator double dielectric loaded waveguides coupled through a five waveguide structure formed by depositing metal fins on each side of the dielectric. The complete structure is inside a waveguide cavity with broadside dimension a and height b. The thickness of each dielectric slab is kept uniform to be d. t is the thickness of the metal septum. W is the distance of the dielectric slab from the center of the cavity. We

are considering a double dielectric loaded section as they offer superior stopband and harmonic suppression than single dielectric loaded structures [39]. The disadvantage of these sections is that, as we increase the number of dielectric slabs in the waveguide cavity the alignment poses a big problem. The length of second resonator sections is comparatively higher than the first resonator section as the amount of coupling required is small.

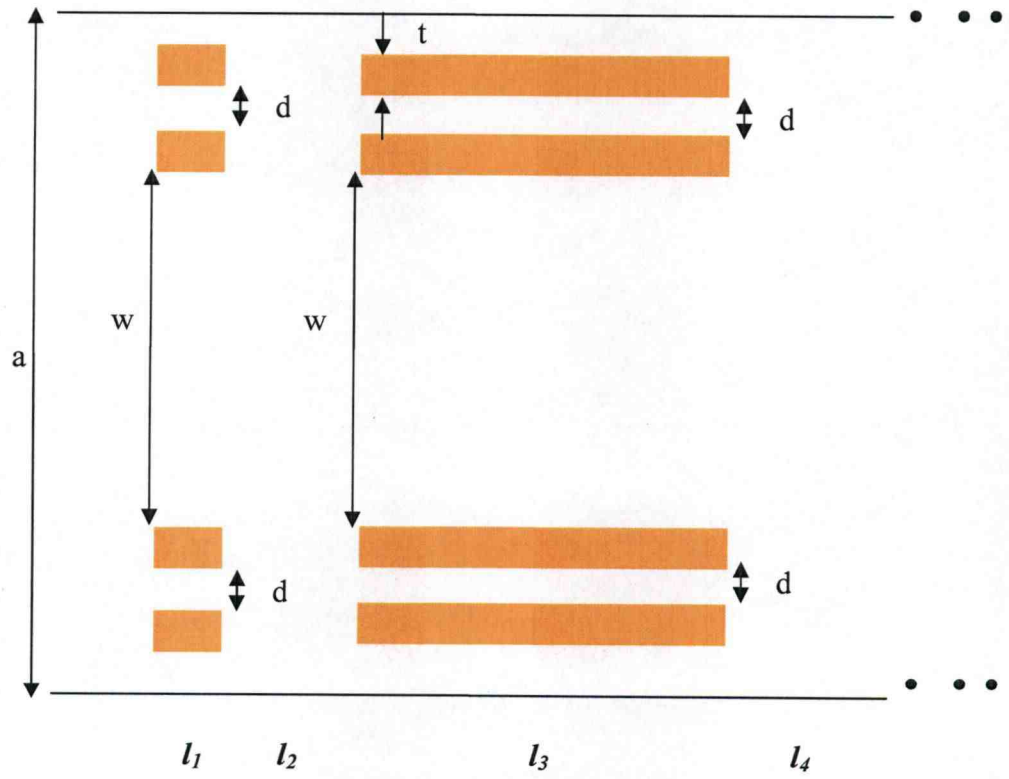

Figure 4.1 A bisected three resonator filter. l_1, l_2, l_3 and l_4 are lengths pertaining to first two resonator sections.

The proposed filter section in Fig 4.2 helps to overcome the shortcomings discussed above by providing an additional degree of freedom to adjust the separation (w) between metal inserts. The dielectric loaded resonators are coupled using five waveguide

structures as reported earlier, but in the newer configurations the slab to center distance i.e. w_1 and w_2 for first and second resonator can be varied to obtain compact geometries. For conventional waveguide-based realization, alignment of metal inserts could be a problem. The proposed filter sections can be easily implemented in multilayer technologies such as LTCC by having via fence to emulate the performance of a metal insert. The effect of varying w_1 and w_2 on section lengths is discussed in the next few sections.

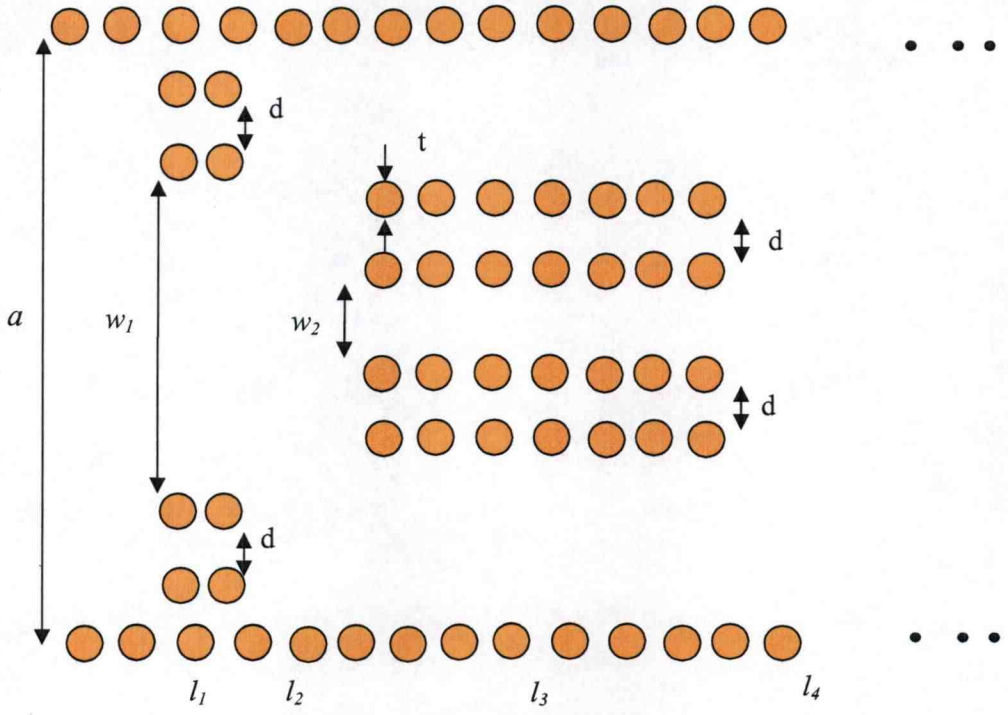

Figure 4.2 A half-filter section of a 3-resonator filter. l_1, l_2, l_3 and l_4 are the lengths pertaining to the first two resonators.

As the waveguide cavity is uniformly filled with dielectric the analysis of five waveguide sections is simplified. The analysis was carried out using the field theory approach discussed in chapter 3 and [39].

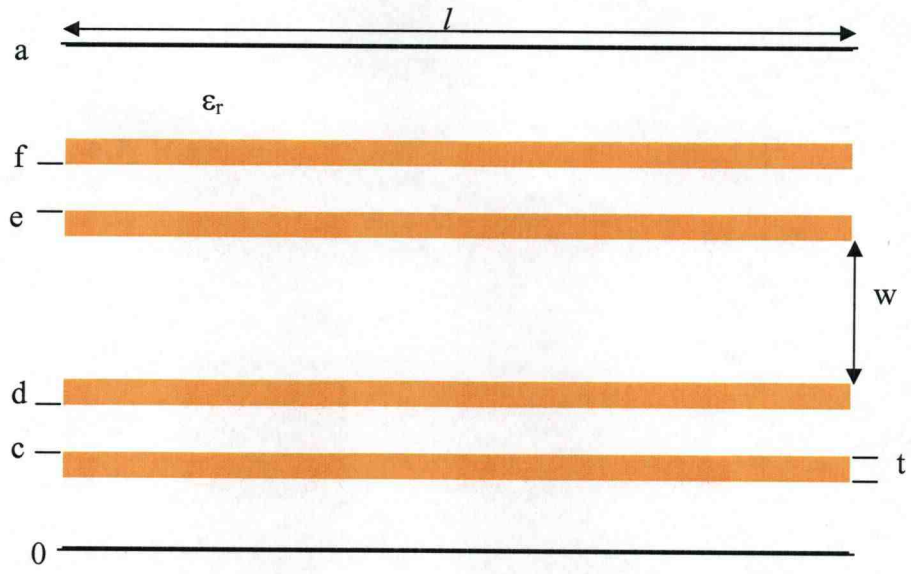

Figure 4.3 Cross Section of a five-waveguide structure

Fig. 4.3 shows the cross section of a 5 waveguide structure. There are 4 conducting layers divide the dielectric loaded waveguide cavity into five waveguide sections. The thickness of each conducting layer is assumed to be t. The length of the section is assumed to be *l*.

4.2 Filter Design

The bandpass filter consists of different sections, the performance of which is determined by the K and ϕ. Fig 4.1(a) shows a filter section for the proposed filters. As can be seen the all sections of the filter are symmetric and is designed using the impedance inverter approach as discussed in chapter 2. The resonator in each of the sections is a five waveguide structure.

The procedure to determine scattering matrix for the filter sections remain the same. Rigorous field analysis undertaking higher mode interactions into effect is carried out.

The resonator sections have been analyzed in the same way as reported in Dr. Settaluri Ph.D. thesis [38].

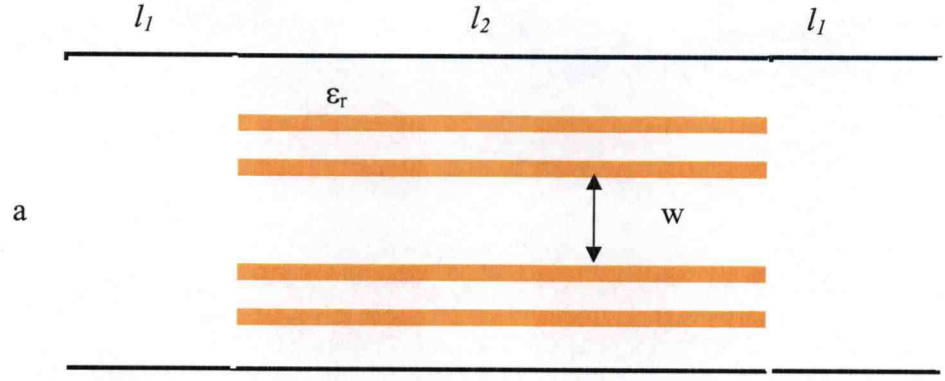

Figure 4.4 Single Filter Section

The typical values of K parameter for first filter section ranges from 0.15 to 0.3 for chebyshev and maximally flat filters designed for bandwidths of 0 to 5 percent with chebyshev ripple of 0.05dB.

4.4 Results

Effect of insert distance from center for first resonator

Fig 4.4 shows the first filter section of the proposed filters. The five waveguide section is symmetric along the center. The first metal inserts in upper half is placed at a distance of w/2. Since there are 4 metal inserts in the waveguide cavity the coupling strength can be varied by adjusting the distance between them. This might lead way to compact filter sections for a given value of coupling coefficient.

Fig 4.5 shows the variation of section lengths for different values of w, as a function of coupling coefficient. It can be observed that shorter filter sections can be obtained for

desired coupling coefficients by varying the separation among the metal inserts. For larger value of coupling coefficient a large separation is required and vice versa.

It can be inferred from the plots in Fig. 4.5 that for a given specifications the length of the filter can be adjusted by appropriately choosing w. The freedom of adjusting the value of w helps designing compact filters unlike conventional waveguides where variation in w might be hard to realize. Table 2 shows three filters designed with the specification of center frequency 29GHz and fractional bandwidth of 0.03 filters with different lengths have been designed using different values of w as shown in fig 4.5. A considerable reduction in filter length can be observed.

Table 8 Section Lengths for a N = 3 bandpass filter

Filter specifications f_o=29 GHz, $\Delta = 0.03$, N = 3, $\varepsilon_r = 2.22$ (Rogers RT Duroid), Maximally Flat response

No.	Section lengths (*mm*)	Total Filter length *(mm)*	b *(mm)*	Section Width (*mm*)
1.	$l_1 = 0.759$ $l_2 = 3.695$ $l_3 = 2.897$ $l_4 = 3.718$	18.42	3.556	$a = 5.0$ $w_1 = 2.5$ $w_2 = 2.5$ d = 0.25 t = 0.25
2.	$l_1 = 0.759$ $l_2 = 3.991$ $l_3 = 1.107$ $l_4 = 4.310$	16.02	3.556	$a = 5.0$ $w_1 = 2.5$ $w_2 = 1.75$ d = 0.25 t = 0.25
3.	$l_1 = 0.759$ $l_2 = 4.048$ $l_3 = 0.759$ $l_4 = 4.424$	15.555	3.556	$a = 5.0$ $w_1 = 2.5$ $w_2 = 1.5$ d = 0.25 t = 0.25

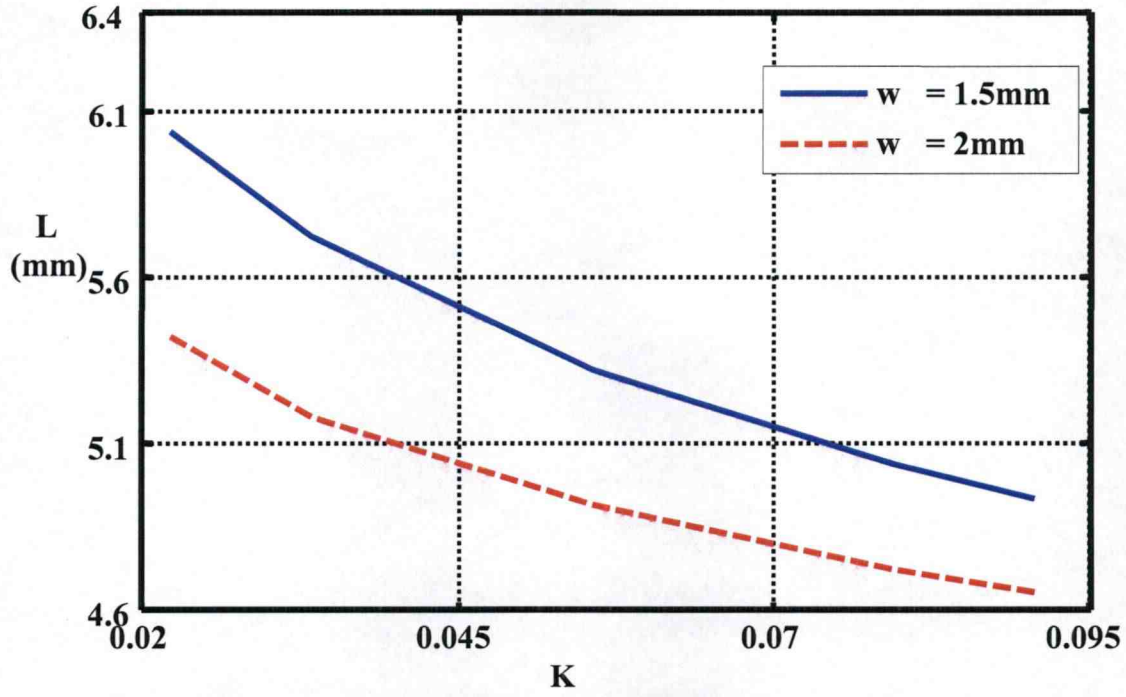

(a) Variation for small values of K. These are typical for second resonator and beyond

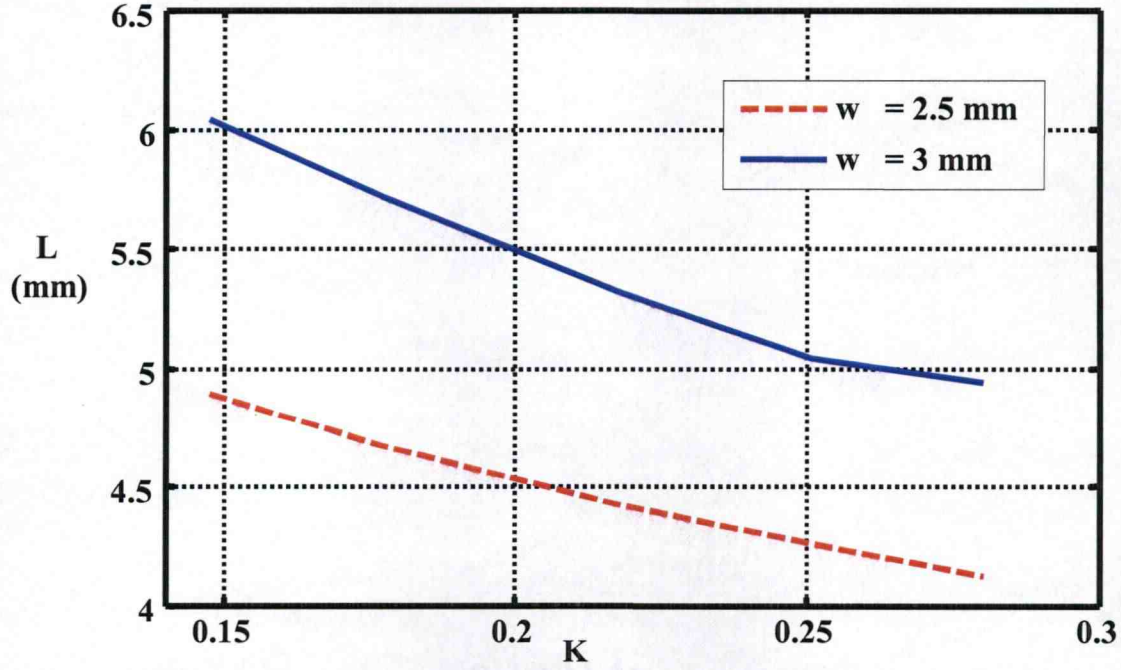

(b) Variation for large values of K. These are typical for first resonator section.

Figure 4.5 Variation in length of a filter section with K for different values of w.

Fig 4.6 shows the simulated frequency response for the three filters superposed in one plot. A 4.5 GHz shift in first harmonic can be observed. The filter with the smallest footprint showed superior characteristics in pass band and stopband. It can be inferred that compact filters can be designed at higher frequencies by smartly choosing the value for w.

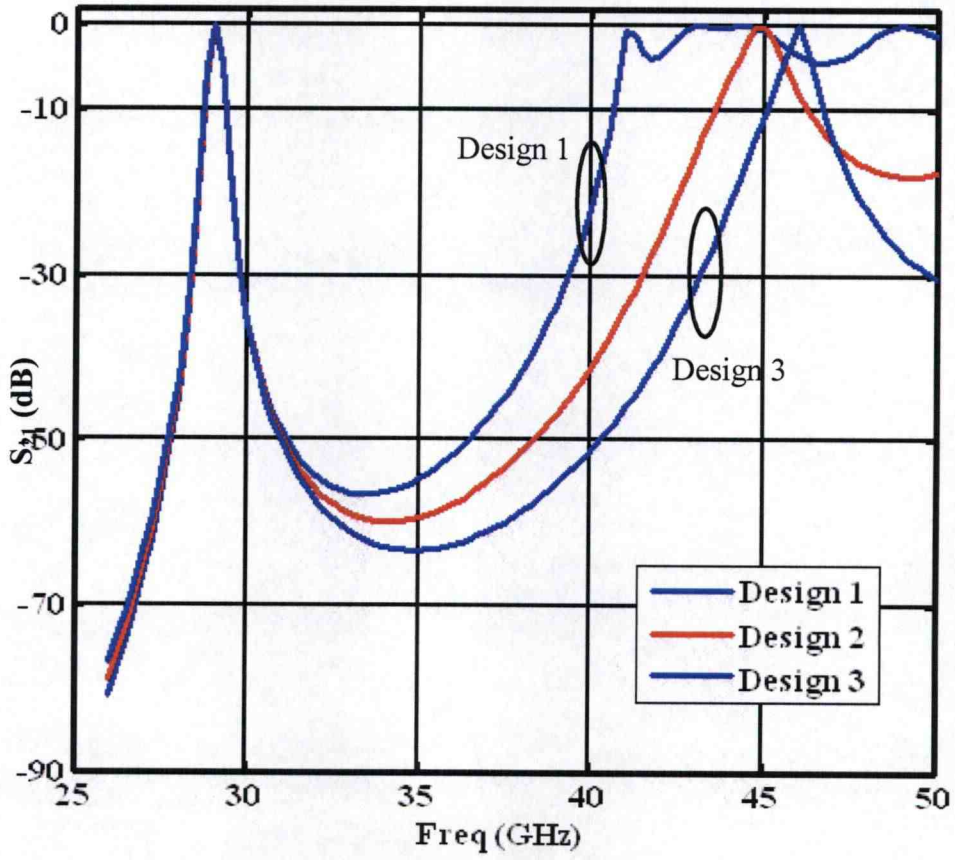

Figure 4.6 Frequency response of filters designed in Table 2

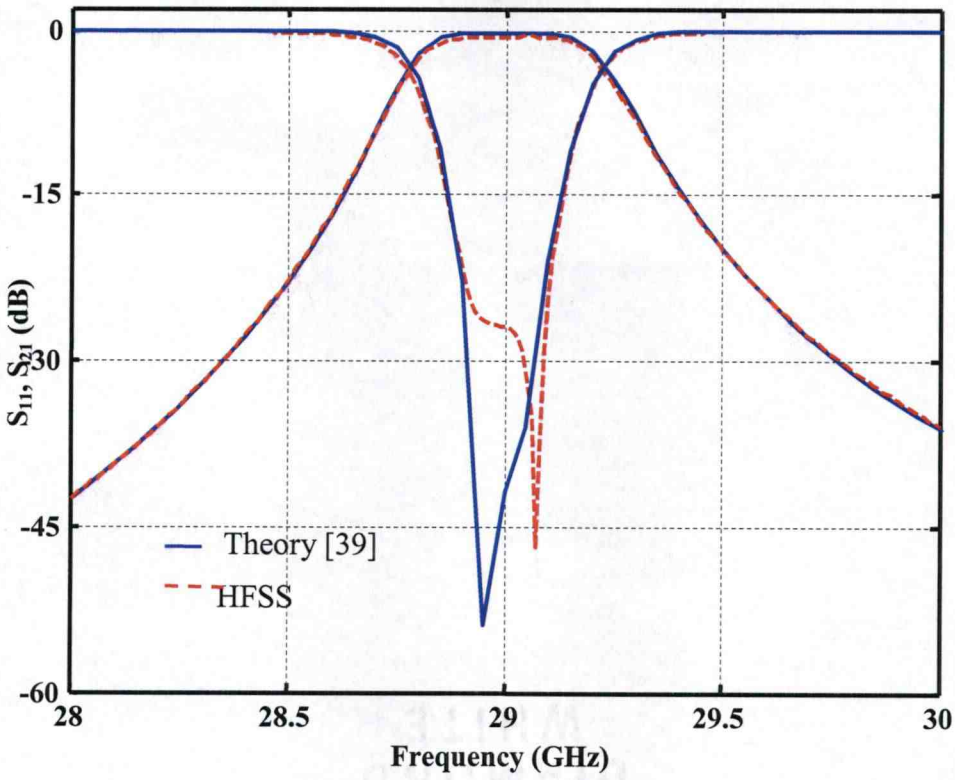

Figure 4.7 Frequency Response for design C from Table 8

Fig. 4.7 shows the frequency response for design C from Table 8. The filter has been designed using analysis technique as explained in [38]. It can be seen that the two frequency response show a close match. It can be inferred from the response that metal-insert filters can be implemented in LTCC technologies. Fig. 4.8a shows three dimensional view of the 3D model and Fig. 4.8b shows the top view of the structure that was simulated in HFSS for design C from Table 8.

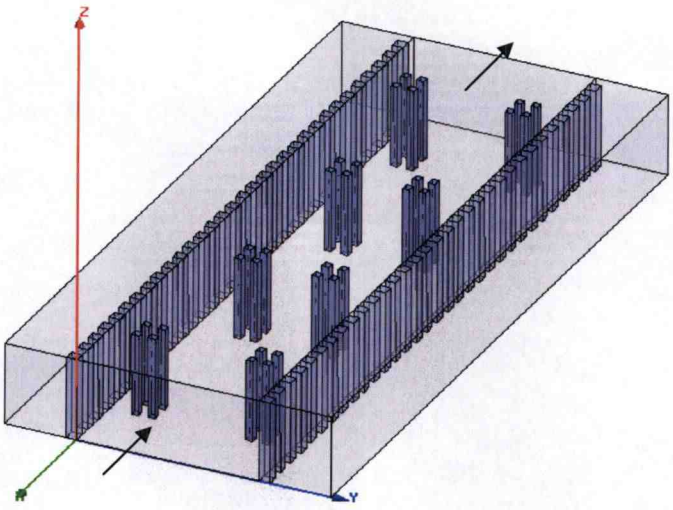

(a) 3D view of the model simulated in HFSS for Design C

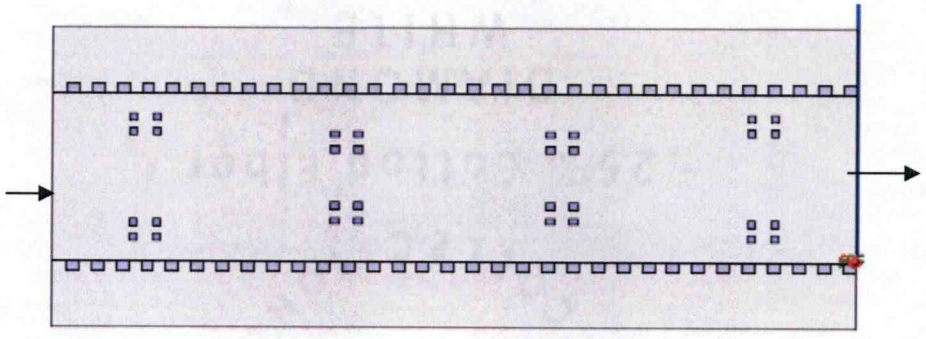

(b) Top view of the model simulated in HFSS for Design C

Figure 4.8 3D model for Design C from Table 8

5. CONCLUSIONS

This chapter describes the highlights of the performed research. A summary and recommendations for future work have also been included.

5.1 Summary

The research focused on developing new configurations of via-only waveguide bandpass filters for application to multi-layered LTCC configurations. Embedded waveguides realized with a series of vias to replace the sidewalls of a conventional rectangular waveguide bridges the gap between waveguide components and available multi-layer technologies. A complex, full-wave field theory analysis combined with impedance inverter equivalent synthesis approach for the design of novel, easy to fabricate, low cost via-only bandpass filters for multi-layered substrates has been presented. Full wave simulations in HFSS have been carried out to validate the theoretical results. A study was carried out to optimize the settings for different simulation parameters in order to optimize the simulation process.

Initial efforts were directed to the design of filters using H-Plane steps. As the research evolved the H-plane filters gave way to inductive iris filters and ultimately an attempt was made to implement the filters in multi-layer configurations using via arrays. The feasibility of the proposed configuration has been demonstrated by designing three filters in Ka, Ku and X bands. The analysis and synthesis approaches followed in this work give a significant reduction in computation times for the proposed configurations. A three resonator filter can be accurately designed using proposed techniques in approximately

10 minutes on a Pentium IV 2.1 GHz processor, 784 MB as opposed to 15 hours in a full wave solver for the same structure.

After successful validation of waveguide inductive iris filter, the approach has been extended to design of E-Plane filters with superior stopband characteristics. Compact filters were designed for the Ka band. The new filters are suitable for multi-layer technologies such as organic substrates and LTCC. The proposed designs should find wide range of applications because of their design simplicity.

5.2 Recommendations

Bandpass filters designed in this work reflect the potential of achieving compact topologies for waveguide based filters in upper microwave and millimeter wave frequencies. Waveguide filters, being widely used in communication systems are well researched and numerous configurations for waveguide based bandpass filters are available in literature. The filters covered in this work are narrowband filters with realization upto 10% fractional bandwidth. As an extension, wideband geometries can be realized using the techniques covered in this thesis. As there is a need of superior stopband characteristics, future work can be aimed at achieving better stopband characteristics and better harmonic suppressions by using asymmetric filter sections at the input.

This work covers all aspects required for successful design of bandpass filters, but the idea of going ahead with the fabrication of these filters will consolidate the analysis and synthesis techniques proposed in this work.

BIBLIOGRAPHY

[1] J.A. Ruiz-Cruz, M.A.E. Sabbagh, K.A. Zaki, J.M. Rebollar, Z. Yunchi, "Canonical ridge waveguide filters in LTCC or metallic resonators," *IEEE Trans. Microwave Theory Tech.*,Vol. 53, pp. 174–182, Jan. 2005.

[2] Y. Rong, K. A. Zaki, M. Hageman, D. Stevens, and J. Gipprich, "Low temperature cofired ceramic (LTCC) ridge waveguide bandpass chip filters," *IEEE Trans. Microw. Theory Tech.*, vol. 47, no. 2, pp. 2317–2324, Feb. 1999.

[3] J. Gipprich, D. Stevens, M. Hageman, A. Piloto, K. A. Zaki, and Y.Rong, "Embedded waveguide filters for microwave and wireless applications using cofired ceramic technologies," in *Proc. Int. Microelectronics Symp.*, San Diego, CA, 1998, pp. 23–26.

[4] Y. Rong, K.A. Zaki, M. Hageman, D. Stevens, J. Gipprich, "Low temperature cofired ceramic (LTCC) ridge waveguide multiplexers," *Microwave Symposium Digest, IEEE MTT-S International*, Vol.2, pp. 1169–1172, 2000.

[5] A. Piloto, K. Leahy, B. Flanick, and K. A. Zaki, "Waveguide filters having a layered dielectric structure," U.S. Patent 5 382 931, Jan. 17, 1995.

[6] V. Govind, S. Dalmia and M. Swaminathan, "Design of integrated low noise amplifiers (LNA) using embedded passives in organic substrates," *IEEE Trans. on Adv. Pkg.*, vol. 27, pp. 79–89, Feb. 2004.

[7] G. Carchon *et al.*, "Multilayer thin-film MCM-D for the integration of high performance wireless front-end systems," *Microwave J.*, vol. 44, pp. 96–110, Feb. 2001.

[8] C. Edward, Niehenke, *P.A.* Robert, I J. Bahl, "Microwave and Millimeter-Wave Integrated Circuits," *IEEE Trans. Microwave Theory Tech.*, Vol. 50, pp. 846–856, 2002.

[9] MF. Davis, A. Sutono, K. Lim, J. Laskar, V.Sundaram, J. Hobbs, G.E. White, R. Tummala, "RF-microwave multi-layer integrated passives using fully organic system on package(SOP) technology," *Microwave Symposium Digest, 2001 IEEE MTT-S International*, Vol. 3, pp.1731–173, May 2001.

[10] D. Stevens, J. Gipprich, "Microwave Characterization and Modeling of Multilayered Cofired Ceramic Waveguides," *1998 Proceedings of the International Symposium on Microelectronics (IMAPS 98)*, San Diego, CA, November 1–4, 1998.

[11] A. Sutono, D. Heo, Y.-J. Emery Chen, J. Laskar, "High-Q LTCC-based passive library for wireless system-on-package (SOP) module development," *IEEE Trans. Microwave Theory Tech.*, Vol. 49, pp.1715 – 1724, Oct. 2001.

[12] Lei Zhu and Ke Wu, "Accurate Circuit Model of Interdigital Capacitor and Its Application to Design of New Quasi-Lumped Miniaturized Filters with Suppression of Harmonic Resonance," *IEEE Trans. Microwave Theory Tech.*, Vol. 48, March 2000.

[13] Sheta A. F, Helta. K., Coupez .J. P, Person. C, Toutain. S, Blot J. P, "A new semi lumped microwave filter structure," *IEEE Trans. Microwave Theory Tech.*, Vol.2, May1995.

[14] Jen-Tsai Kuo, Wei-Hsiu Hsu, and Wei-Ting Huang, "Parallel Coupled Microstrip Filters with Suppression of Harmonic Response," *IEEE Microwave and Wireless Components Letters*, Vol. 12, No.10, 0ctober 2002.

[15] Lei Zhu and Ke Wu, "Field Theory-based Design and Optimization of compact Multiple Gap Coupled Microstrip Filter with Loaded Stub," Proceedings of the Asia Pacific Microwave Conference, 1997.

[16] J.A. Curtis, S.J. Fiedzuszko, "Multi-layered planar filters based on aperture coupled, dual mode microstrip or stripline resonators," *IEEE MTT-S, Digest*, 1992. pp. 1203–1206.

[17] J.S. Hong, M.J. Lancaster, "Back-to-back microstrip open-loop resonator fitlers with aperture couplings," *IEEE MTT-S Digest*, 1996, pp. 1239–1242.

[18] R. K. Settaluri, A. Weisshaar, and V.K. Tripathi, "Design of Compact Multilevel Folded-Line bandpass filters," *IEEE Trans. Micro. Theory Tech.*, Vol. 49, pp.1804–1809, Oct. 2001.

[19] Kala Gururajan, Harish Peddibhotla and Raghu K. Settaluri, "New Configurations of Single and Multi-Level Bandpass Filters with Excellent Harmonic Suppression," *Micro. Optical. Tech. Letters*, Vol. 39, pp. 490–493, Dec. 2003.

[20] R.K. Settaluri, K. Gururajan, "EM Based Design of Square-ring Vialess Bandpass Filters,"

[21] Kuo. J. T, Shih.E, "Microstrip stepped impedance resonator bandpass filter with extended optimal rejection bandwidth," *IEEE Trans. Micro. Theory Tech.*, Vol. 51, 2003.

[22] F. Arndt, J. Bornemann, D. Grauerholz, and R. Vahldieck, "Theory and Design of Low-Insertion Loss Fin-Line Filters," *IEEE Trans. Micro. Theory Tech.* Vol. 30, pp.155-163, 1982.

[23] F. Arndt, J. Bornemann, "Rigorous design of Evanescent – Mode E- Plane Finned Waveguide Bandpass filter," *IEEE Trans. Micro. Theory Tech.* Vol. 37, pp.603 - 606, 1989.

[24] R. Vahldieck, J. Bornemann, F. Arndt, and D. Grauerholz, "Optimized waveguide E-plane metal inset filters for millimeter- wave applications," *IEEE Trans. Micro. Theory Tech.*, vol. MTT- 31, pp. 65 - 69. Jan. 1983.

[25] R. Vahldieck, W. Hoefer, "Finline and Metal Insert Filters with Improved Passband Separation and Increased Stopband Attenuation", *IEEE Trans. Micro. Theory Tech.*, vol. MTT- 33, pp. 1333-1339. Jan. 1985.

[26] D. Budimir, "Optimized E-Plane Bandpass Filters with Improved Stopband Performance," *IEEE Trans. Micro. Theory Tech.*, vol. MTT- 45, pp. 212 - 220. Jan. 1997.

[27] W. Menzel, f. alessandri, M. Mongiardo, R. Sorrentino, c. Eswarappa, P.P.M.so, and W.J.R. Hoefer, " Analysis of a millimeter-wave filter using transmission line matrix and mode matching methods and comparision with the measurements," *in Proc. 9th Annu. Rec. Progress Appl. Computational Electromgn*, Monterey, CA, Mar. 1993, pp. 286-296.

[28] A. Weisshaar, M. Mongiardo and V. K. Triapathi, "Full-Wave Computer Aided Design of Waveguide Components by Circuit Simulation.," Wiley, 1998. pp. 236-246, 1998.

[29] H.Uchimura, T. Takenoshita, M.Fuji, "Development of a laminated waveguide," *IEEE Trans. Microwave Theory Tech.*, vol. 46, pp. 2438–2443, Dec. 1998.

[30] W.Y.Leung, K.K. Cheng and K.L.Wu, "Multi-layer LTCC bandpass filter design with enhanced stopband characteristics," *IEEE Microwave and Wireless Component Letters*, Vol. 12, pp. 240-242, July 2002.

[31] Y. Huang, K.L. Wu, "A Broad-Band LTCC Integrated Transition of Laminated Waveguide to Air-Filled Waveguide for Millimeter-Wave Applications," *IEEE Trans. Microwave Theory Tech.*, vol. 51, pp. 1613–1617, May 2003.

[32] Y. Huang; K.L Wu; M. Ehlert, "An integrated LTCC laminated waveguide-to-microstrip line T-junction," *Microwave and Wireless Components Letters, IEEE [see also IEEE Microwave and Guided Wave Letters]*, Vol. 13, pp.338 – 339, 2003.

[33] *High Frequency Structure Simulator, HFSS v.9.2,* Ansoft corporation.

[34] G. Matthaei, L. Young and E.M.T. Jones, *Microwave Filters, impedance-matching networks, and Coupling Structures*, Artech House Publishers, 1980.

[35] N. Marcuvitz, *Waveguide Handbook.* Stevenage: IEE, 1986,

[36] D.M. Pozar , *Microwave Engineering*

[37] A. Weisshaar, M. Mongiardo, A. Tripathi and V. K. Triapathi, "CAD – Oriented FullWave Equivalent Circuit models for Waveguide Components by Circuits," *IEEE Trans. Micro. Theory Tech.*, vol. MTT- 44, pp. 2564-2570. 1996.

[38] G.Bhargava, R.K. Settaluri, "Microwave/Millimeter Wave Via-Only Bandpass filters for LTCC Applications," *IEEE.*

[39] R.K. Settaluri, "Double Dielectric Fin-Lines and E-Plane Filter for Millimeter Wave Applications," Ph.D. Thesis.